
INTERMITTENT CONTROL AS A MODEL OF MOUSE MOVEMENTS

J. Alberto Álvarez Martín
James Watt School of Engineering
University of Glasgow, Scotland.
alberto.alvarez-martin@glasgow.ac.uk

Henrik Gollee
James Watt School of Engineering
University of Glasgow, Scotland.
hernik.gollee@glasgow.ac.uk

Jörg Müller
Institute for Computer Science
University of Bayreuth, Germany.
joerg.mueller@uni-bayreuth.de

Roderick Murray-Smith
School of Computing Science
University of Glasgow, Scotland.
roderick.murray-smith@glasgow.ac.uk

ABSTRACT

We present Intermittent Control (IC) models as a candidate framework for modelling human input movements in Human–Computer Interaction (HCI). IC differs from continuous control in that users are not assumed to use feedback to adjust their movements continuously, but only when the difference between the observed pointer position and predicted pointer positions become large. We use a parameter optimisation approach to identify the parameters of an intermittent controller from experimental data, where users performed one-dimensional mouse movements in a reciprocal pointing task. Compared to previous published work with continuous control models, based on the Kullback-Leibler divergence from the experimental observations, IC is better able to generatively reproduce the distinctive dynamical features and variability of the pointing task across participants and over repeated tasks. IC is compatible with current physiological and psychological theory and provides insight into the source of variability in HCI tasks.

Keywords Human-computer interaction, control theory, modelling, pointing, intermittent control

1 Introduction

One of the most important areas of study of Human-Computer Interaction (HCI) is how humans can interact with computers to input information into computers or control their state. Most applied human–computer input is via activity of the user’s neuromuscular system causing movement of their body, which is sensed by input devices and produces a change in the state of the computer. The most widely-studied example of this in HCI is mouse movement, where a user’s hand moves a mouse to change the cursor position. The goal of this article is to provide a physiologically plausible model of such user movements and the associated movement variability. While our long-term objective is to understand movement during interaction with computers in general, in this paper we focus on a simple core task: aimed movements of a mouse cursor towards a static target of a certain width at a certain distance.

Movement in interaction with computers is inherently dynamic and clearly happens in a feedback loop. Users observe the current state of the computer (e.g., cursor position) and adjust their movements to change this state into the state they desire – *“movements only make sense when they are precisely located in time and space that is, when they are part of an action, seeking to accomplish a goal. In this sense, simple goal-directed movements, such as pointing and grasping, can be considered to be the building blocks of more complex actions”* (Bootsma et al., 2004). Control theory is the mathematical framework for systems with feedback which are achieving specific objectives, and its relevance for HCI is reviewed in (Murray-Smith, 2018) and (Müller et al., 2017).

In this paper we explore the benefits of interpreting interaction with computers as intermittent control. In intermittent control, open-loop control trajectories are generated based on an internal estimate of the state of interactions using a predictive model of how this state will evolve over time. The open-loop trajectories are intermittently updated with feedback information from continuous observations of the systems. Only if the observed state deviates from

the predicted state, do they update their prediction and control accordingly. Loram et al. (2014) explain why the intermittent control perspective is more physiologically plausible as an explanation of human motor control than our previous continuous control perspectives of interaction with computers (e.g., (Müller et al., 2017)). It has been shown that humans are generally not able to adjust their movement continuously (Navas and Stark, 1968). The switching and intermittency inherent in Intermittent Control provides a powerful explanation of the source of variability in human movement, and potentially, it can also explain the emergence of phenomena that are difficult to explain from a continuous control perspective, such as submovements.

1.1 Beyond Fitts’ law

Since the advent of graphical user interfaces, aimed movements towards a spatially defined target have become a primary means of input to computers. It is well known that all movements involve variability in their performance. For aimed movements, this has been described in the “speed-accuracy tradeoff”, modelled through Fitts’ law (Fitts, 1954). Fitts’ law allows the prediction of movement time MT as a function of distance D to and width W of the target, as $MT = a + b \log(D/W + 1)$ in the Shannon formulation (MacKenzie, 1992). The application of Fitts’ law to understand interaction with computers is often viewed as one of the greatest successes of the field of HCI (Guiard and Beaudouin-Lafon, 2004a). Fitts’ law allows for the model-based evaluation of user interfaces, reducing the number of necessary user tests, and serves in the automatic optimization of user interfaces such as GUI layouts or keyboards. Perhaps most importantly, it has sharpened the intuition of generations of user interface designers about the role of the users’ motor control processes in interaction with computers.

One of the strengths, but also limitations, of Fitts’ law is that it reduces the complexity of human movement to a single number, the movement time, but it makes no testable predictions about the process of the movement. The Fitts’ law perspective offers no explanation of the causal relationship that links conditions and outcomes in pointing. Neither the biomechanical, perceptual and cognitive properties of the human nor the properties of the computer interface such as input sensors, delays, jitter or style of feedback can be understood from this perspective. It does not allow any understanding of *why* a certain user interface, interaction technique or input device is better than another. In particular, the trajectory of the pointer, velocities and accelerations can not be explained by Fitts’ Law, so a richer understanding of the broader process of movement is lost, and as (Bootsma et al., 2004) observe, “*while the duration of movement constitutes a particularly pertinent global measure of behavior, useful in many different contexts, it does not allow a full appreciation of the processes underlying behavioral organization. In the domain of perceptuomotor control, it is widely accepted that a more fine-grained window into these processes is available through the kinematics of movement*”. Perhaps most critically, Fitts’ law is limited to aimed movements. This may make it more difficult for the field of HCI to think beyond aimed movements and point-and-click as the foundation of interface design. In order to develop a deeper understanding in HCI of how users create input to computers by moving their bodies, we propose that we need to take a control theoretic perspective, and we are exploring models which are appropriate for the representation of purposeful human movement.

1.2 Paper structure

In this paper, we present a model of aimed mouse movement in the interaction with computers, based on intermittent control. We build on an existing dataset to fit the parameters of our event-driven intermittent controller, allowing a comparison with the continuous implementations proposed in (Müller et al., 2017). The objectives of this paper are:

1. To identify the parameters of an intermittent controller from the experimental mouse movement data by using an optimisation approach.
2. Examine the ability of IC to generatively reproduce and explain distinctive dynamical features of the pointing task such as the velocity profile and the variability observed across participants.
3. Introduce IC as a plausible framework to understand and model user movement in the interaction with computers, as a novel analytic and practical tool for HCI research and practice.

The content of the paper is organised as follows: After reviewing related work in Section 2, a general introduction to the IC framework is given in Section 3, focusing on its role in pointing and human variability. We highlight that the model is based on human physiological insight, and includes predictive properties which are key to understanding and modelling human behaviour in interaction contexts. Section 4 then provides a more mathematically formal description of the theoretical details of IC. Section 5-7 provide descriptions of the experimental dataset and the models and optimisation process used for the analysis. Section 8-9 provide the modelling results, demonstrating that Intermittent control models provide improved modelling of the variability and dynamics of mouse movements compared to previous publications. In Sections 11 and 12 we discuss the conceptual and practical advantages of the model, and give an outlook on further developments.

2 Related Work

2.1 Fitts' Law and Information Theory

Since the original work (Fitts, 1954), Fitts' relationship has been used in a wide range of HCI-relevant publications. For more background, Guiard and Beaudouin-Lafon (2004b) introduce a special issue celebrating 50 years of Fitts' law and Soukoreff and MacKenzie (2004) review 27 years of Fitts' law in HCI and makes recommendations to HCI researchers wishing to construct Fitts' law models for movement time prediction, or for the comparison of conditions in an experiment. Wobbrock et al. (2008) show that Fitts' law implies a predictive error rate model, and that the effect on error rate of target size W is greater than that of target distance D .

Dynamic aspects of Fitts' law task are explored in (Billon et al., 2000; Bootsma et al., 2004; Guiard, 1993), and (Jagacinski, 1977; Jagacinski and Flach, 2003) link Fitts' law models to first and second order control models. While most Fitts' law experiments are artificial lab studies, Chapuis et al. (2007) collected kinematic data from 24 users over several months as part of their normal interactions with a computer. Some papers have explored dynamic relationships in implementations of motor and display spaces, while not taking an explicitly control-theoretic perspective. While pointing in the physical world is constrained by physical laws, Balakrishnan (2004) observed that pointing in the virtual world does not have to abide by the same constraints, and compared approaches aiming to 'beating' Fitts' law by artificially reducing the target distance, increasing the target width, or both, essentially adapting the dynamics of the control task. Blanch et al. (2004) introduced the concept of *Semantic pointing*, which manipulates control-display gain, using two independent sizes for targets in motor space, adapted to its importance for the manipulation, and in visual space, adapted to the amount of information it conveys. Their experimental results suggested that the performance of semantic pointing is given by Fitts' index of difficulty in motor rather than visual space.

2.2 Study of Movement from an intermittent perspective

Control of body movements has been modelled as both discrete and continuous processes, and there are strong arguments for either perspective:

In favour of the **continuous perspective**, the human hand is a physical inertial system, which changes its position smoothly over time. Although difficult aimed movements can be segmented into submovements, identifying the beginning and end of submovements is notoriously difficult. In some movements, there do not seem to be submovements at all. The continuous perspective can also explain other movements which are not aimed movements, such as following a moving target, steering a cursor along some path, controlling a character or vehicle in a video game, etc. Understanding movement as a series of discrete submovements does not appear to concisely capture these phenomena.

In favour of the **discrete perspective**, data shows that humans are not capable of continuously controlling their movements in the same way as an engineered continuous control system. Craik first reported this in (Craik, 1947, 1948). In particular, the *psychological refractory period* (Telford, 1931) dictates that humans can not react to further changes in the environment for a certain time after they reacted to a change: The reaction onset to a second stimulus which follows shortly after the first is delayed as the human is refractory during this time. Crucially, a control paradigm based on continuous feedback is unable to explain refractoriness in human motor control.

Interestingly, the perspectives of discrete movements vs. continuous control may be less contradictory than it first seems. Craik, proposed that a series of discrete movements could appear to be continuous in nature. From this perspective, the human hand moves continuously, but the way the hand moves is only changed at certain points in time, or *intermittently*. Craik's manual tracking experiments led to the conclusion that the human operator uses an intermittent approach, dictated by refractoriness, when tracking discrete reference steps, and that manual control can be seen as the execution of discrete actions that are computed based on the available sensory information and applied as individual open-loop trajectories that are not modified by feedback until completed. Since then, intermittency from the perspective of human motor control has been studied extensively by the physiology community (Navas and Stark, 1968; Nielson, 1999; Loram and Lakie, 2002; Oytam et al., 2005; Loram et al., 2006), and as consequence, computational frameworks have been developed to model the human operator as an intermittent controller using concepts of modern control theory. On the engineering side, the intermittent controller has its origins in the implementation of model-based predictive control (MPC) in the presence of hard constraints (Ronco et al., 1999) and the observer-predictor-feedback architecture from Kleinman (1969) and (Kleinman et al., 1970). It is important to note that, as explained above, intermittency can masquerade as continuous control, in particular when controlling an inertial system, and when the controller has a good internal model of the system (Gawthrop et al., 2011).

Schmidt's Law (Schmidt et al., 1978) addresses variability and dynamics by manipulating amplitude and movement time and measuring the effective target width W_e , leading to the relation $W_e = k \frac{W}{MT}$. The insight behind Schmidt's Law is that the human controls movement via discrete force impulses and the overall variability is from the variation

of the magnitude and duration of the applied force. Meyer et al. (1988) and Meyer et al. (1990) further developed this to the *optimised dual-submovement model* which is consistent with both Schmidt's and Fitts' laws, with the variability of submovements being proportional to the average velocity and that variability leading to the requirement of multiple sub-movements optimised to minimise the total movement time. The assumption being that subjects move to the target region as quickly as possible, while maintaining a high proportion of target hits. To achieve that, they need to cope with the variability induced by motor noise.

The *Iterative Corrective Submovements* model proposed by Crossman and Goodeve (1983) is a model where an aimed movement is understood as a series of individual submovements towards the target, each with a constant error and constant duration. Crossman and Goodeve show how Fitts' law can be derived from this model.

In HCI, movement is also often understood as a series of events, such as submovements, and the Crossman and Goodeve model is widely used. This includes well-known HCI models, such as the work by Card et al. (1986), who introduced their 'GOMS' framework where a Model Human Processor represented movement as a series of discrete steps. However, Crossman and Goodeve (1983) also presented an alternative continuous explanation of aimed movements, that predicts the position of the hand at any point in time, during the movement.¹

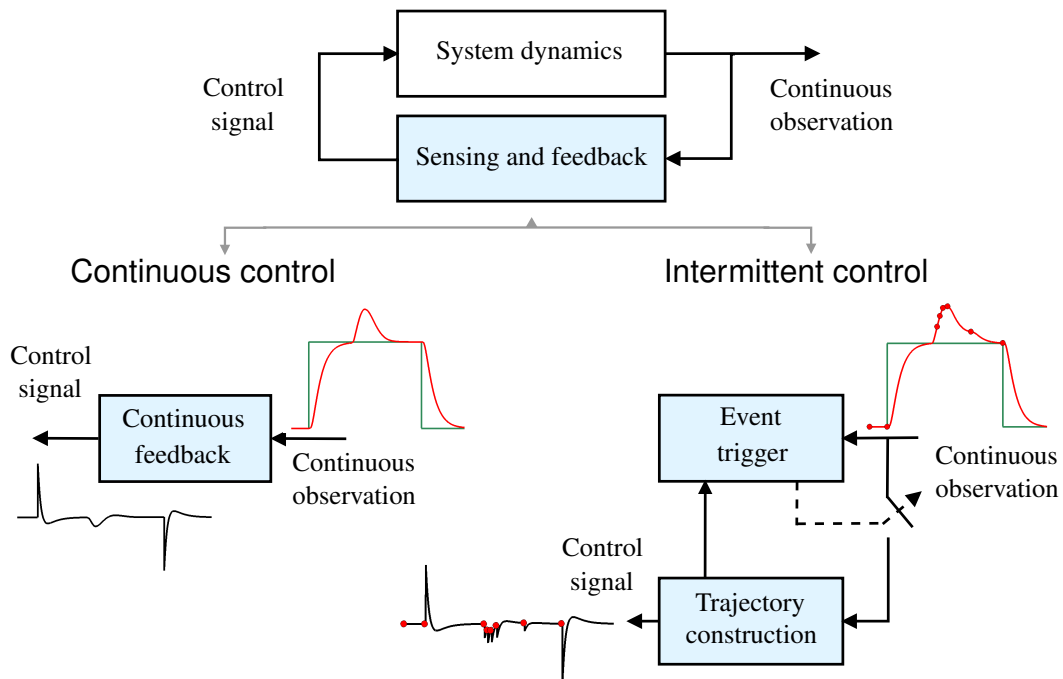


Figure 1: Feedback control: continuous and intermittent control. The top diagram shows a generic control loop: Feedback can be used to control the behaviour of a dynamic system, which involves “sensing” relevant variables to form a representation of the system’s state, before generating a control signal based on a feedback control law. In continuous control (bottom left block diagram), the control signal (time-series in black) is generated continuously, based on observations of the system (time-series in red). In intermittent control (bottom right), feedback information from continuous observations is only used intermittently (determined by an *event trigger*) to reset an open-loop control signal trajectory. The instances when feedback is used in intermittent control are indicated by circles on the red and black time-series, representing the system output and the control signal, respectively. The control signal trajectories between two consecutive red circles (or *events*) are generated open-loop, i.e. without the use of feedback.

2.3 Intermittent Control

Feedback control involves applying a control signal to a dynamic system, based on observations which are combined into an estimate of the system’s state (“sensing”), and a feedback law, cf. Fig. 1. In the traditional continuous control

¹Interestingly, this first-order-lag model (IOL) of movement seems to be less well-known in HCI than the Iterative Corrective Submovements model presented in the same paper. The IOL assumes that the user is continuously observing the cursor position, and adjusts the velocity of the mouse as a constant fraction of the distance of the cursor to the target. Crossman and Goodeve also show how Fitts' law can be derived from this different model.

paradigm (bottom left in Fig. 1), the control signal is continuously adjusted using continuously observed information. In contrast, intermittent control (IC), as introduced in (Gawthrop and Wang, 2009; Gawthrop et al., 2011, 2015), and shown in the bottom right of Fig. 1, employs an event-trigger to switch between closed-loop and open-loop configurations, using feedback at only specific moments in time to generate an control trajectory that is then applied during the open-loop interval, where there is no feedback.

There are strong theoretical and practical modelling motivations for the use of IC in human motor control. It has recently been shown that refractoriness can also be observed in more complex human control tasks (van de Kamp et al., 2013), and that a control strategy which applies feedback only intermittently can successfully model this phenomenon (Loram et al., 2012). The physiological basis for muscle activity in human motor control is also a motivation for the use of intermittent models, and provides insight into the source of variability in human control of input devices (Gollee et al., 2017). Intermittency can serve as a mechanism to modulate the relationship between exploration and exploitation or, in other words, the stability and plasticity trade-off that is critical for adaptation and learning in human behaviour (Loram et al., 2015). When humans learn to control something new, such as a mouse, they need to build an internal model of the dynamics of what they are controlling. In particular, they need to identify parameters of such an internal model from interaction with the device, ie. in a closed-loop setting. In any situation where we are trying to identify model parameters from noisy data acquired in a closed-loop setting, there are problems of bias in parameters due to the correlations between input and output induced by the feedback (Forssell and Ljung, 1999). The intermittent breaking of the feedback loop in IC allows model parameter fitting without the correlated noise from feedback affecting the estimates.

Previous applications of IC in human motor control were mostly interested in how humans can move their bodies from a physiological perspective, so aimed movements were mostly investigated with the bare hand, or with absolute control devices such as joysticks. This paper is the first application of the formal IC framework to mouse movements in an HCI context. The mouse provides only a relative mapping between mouse movements and pointer movement, considerably complicating the control mapping. For these reasons, pointing with the mouse has been investigated very rarely in the field of human motor control. In contrast, mouse movements are at the heart of the field of Human-Computer Interaction, looking at situations where humans control the state of a computer system, via potentially complicated mappings.

2.4 Control of Computers

Traditionally, HCI is often presented as *communication of information* between the user and computer, and has used information theory to represent the bandwidth of communication channels into and out of the computer via an interface, but this does not provide an obvious way to measure the communication, or whether the communication makes a difference. Information theory *alone* is not sufficient as a framework for modelling HCI.² Humans often want to control some aspect of the world (e.g. the temperature in a room, or the volume of a music player) via a computer, or change the state of a computer in its own right. In either case we have a dynamic feedback loop which passes through a computer, where in order to communicate the simplest symbol of intent, we typically require to move our bodies in some way that can be sensed by the computer, often based on feedback while we are doing it. Our bodies move smoothly through space and time, so any communication system is going to be based on a foundation of continuous control. However, inferring the user's intent is inherently complicated by the properties of the control loops used to generate the information – intention in the brain becomes intertwined with the physiology of the human body and the physical dynamics and transducing properties of the computer's input device, as well as the brain's own predictions of these aspects. We therefore have sensitivity to both variability of human motor control execution, and need to take user predictions about their own behaviour into account, highlighting the role of the model-predictive intermittent control methods explored in this paper.³ Murray-Smith (2018) gives an overview of the role of control theory in the study of HCI and (Jagacinski and Flach, 2003) provide a readable introduction to control and dynamics concepts for non-engineers.

Control theory provides an engineering framework which is well-suited for analysis of closed-loop interactive systems. This can include properties such as feedback delays, sensor noise (see e.g. (Trendafilov and Murray-Smith, 2013)), or interaction effects like 'sticky mouse' dynamics, isometric joystick dynamics (Barrett et al., 1995), magnification effects, inertia, fisheye lenses, speed-dependent zooming, all of which can be readily represented by dynamic models. The use of state space control methods was explored in document zooming context in (Eslambolchilar and Murray-Smith, 2004, 2006, 2008; Kratz et al., 2010) and Quinn et al. (2013) reviewed the challenge of optimising touch

²Julien Gori has been updating the information theoretic analysis of Fitts' law tasks in (Gori, 2018) and in (Gori et al., 2018) highlighted the potential benefits of including feedback in the analysis.

³Note the similarity to issues in the *Joint cognitive systems* community, where (Hollnagel, 1999; Hollnagel and Woods, 2005) argue that we need to focus on how the *joint* human-computer system performs, not on the communication between the parts.

scrolling transfer functions and used a robot arm to identify the dynamics of commercial products. Examples of the use of dynamic models in interactive dynamic scrolling systems are now widespread in commercial systems, and examples in the academic literature, include (Williamson et al., 2007; Cho et al., 2007). Highlighting the relevance of knowledge of variability in user movements, Quinn and Zhai (2018) used control models to understand how input trajectories associated with words entered into gesture keyboards are likely to vary.

The control perspective can also inspire unusual approaches to interaction, such as *motion pointing* interfaces which infer the user’s intent based on detection of control behaviour, as originally developed by Williamson and Murray-Smith (2004) and built on by Fekete et al. (2009) and, via eye tracking, in a number of applications described in (Velloso et al., 2017). Improved estimation of variability in closed-loop control behaviour would increase the performance of many of these approaches significantly, as they rely on measurement of the divergence of distributions. Motion pointing requires a good model of the user’s ability to perform certain actions. Recent interest in the relevance of detailed inverse biomechanical simulation in HCI includes (Bachynskyi et al., 2015; Bachynskyi, 2016), while Fischer et al. (2020) explores forward biomechanical simulation to simulate pointing movements.

In (Müller et al., 2017) we presented and compared several manual control models of mouse pointing identified from the same mouse movement data used in this paper. These models are generative, estimating not only movement time, but also pointer position, velocity, and acceleration on a moment-to-moment basis. The continuous control models tested captured some of the important dynamic characteristics, but did not explain the variability shown in the data, which led to a poorer fit for low index of difficulty (ID) targets. The models included continuous second order dynamics models, and Costello’s surge model, which has a switching characteristic.

The switching characteristic separates the movement into an open-loop initial surge phase and a later continuous current control phase. This switching behavior has also been modelled by Aranovskiy et al. (2016) and further in (Aranovskiy et al., 2020). Based on the optimised dual-submovement model and the surge model they develop a two-phase model that takes into account nonlinear pointing transfer functions (PTF) which map from mouse movement to cursor movement. While the ballistic movement phase only has access to proprioceptive feedback for control, the following corrective movement phase is guided visually from the pointer position which is mediated by the PTF. The switch between ballistic and corrective movement phase happens at a predefined distance from the target after a transition period with zero acceleration. Aranovskiy et al. derive the exponential stability of the model under some mild assumptions about the PTF, and validate the model against experimental data of reciprocal pointing in the case of a constant gain function. In contrast to the intermittent control model presented in this paper, the model of Aranovskiy explicitly models pointing with a possibly non-constant PTF. On the other hand, the intermittent control model explicitly models intermittency of the control process, the observer and predictive capability of the human, the dynamics of the neuromuscular system, as well as noise and delay in the nervous system. Being based on physiological principles of motor control, the intermittent control model has the potential advantage that it is applicable to a range of movement tasks other than mouse movement.

The *Intermittent Click Planning Model* (ICP) of Park and Lee (2020) describes the process by which users plan and execute optimal click actions, from which the model predicts the pointing error rates for target tracking tasks. Their ICP model assumes that the user is an intermittent controller, following on from the intermittent BUMP model described in (Bye and Neilson, 2008). The main difference between our approach and the BUMP model is that in this paper we use an event-trigger, leading to a variable distribution of open-loop intervals, whereas the BUMP model are based on a constant intermittent interval. Physiological evidence suggests that the open-loop interval is not constant, so an event trigger should be the more reasonable explanation from Gawthrop et al. (2014). The ICP model also assumes that the user is a statistical encoder that makes optimal use of the externally provided information that allows for estimation of click timings. More complex threshold functions for IC are an interesting opportunity for future research.

3 Overview of the intermittent control Model

This section provides an explanation of the main elements in IC with an emphasis on human motor control and integrates them in the form of a unified control model. The purpose is to relate the function of fundamental features of human control in pointing and tracking tasks with classical control theory concepts, while highlighting the differences between IC and a continuous control point of view.

In this context, the flow of information is represented by *signals* (such as the pointer position or motor control signals within the user) that are used as *inputs* to specific *systems* (such as the computer or the biomechanics of the user), and depending on the role of the system, different *outputs* are generated. In human motor control and HCI there are many operations involved in classic tasks that have a direct representation in control theory; for instance, for pointing tasks where the goal is to reach a target using a pointer device of some sort, the target can be seen as a *reference* signal

that should be introduced to the model (Müller et al., 2017). This signal allows the calculation in real-time of the *error* between the target position and the pointer position. In most systems, the goal is to reduce this error as much as possible and a common way to achieve this is by using *feedback*, which means that the output signal delivered by the system we are trying to control is used as an input to a *controller* that computes and applies a correcting signal to the same system. For human in-the-loop systems, this process happens when the system output, such as the display content, is sensed, processed and integrated via our sensory stream, to form an internal representation of the task in the brain (Wolpert et al., 1998; Shadmehr and Mussa-Ivaldi, 2012), meaning that the central nervous system (CNS) uses a combination of prior and present sensory information to estimate internal and external states that are relevant to the task (Bays and Wolpert, 2007), such as pointer position and velocity. This internal representation provides the capability to predict how the system output will behave in the future based on its current state, while cancelling the effects of common delays that affect the transmission of these signals through our neural pathways (Miall et al., 1993; Gawthrop et al., 2011) or within the computer, to then combine all the available information in order to generate control commands, which cause the muscles to contract in a way to achieve the desired effect.

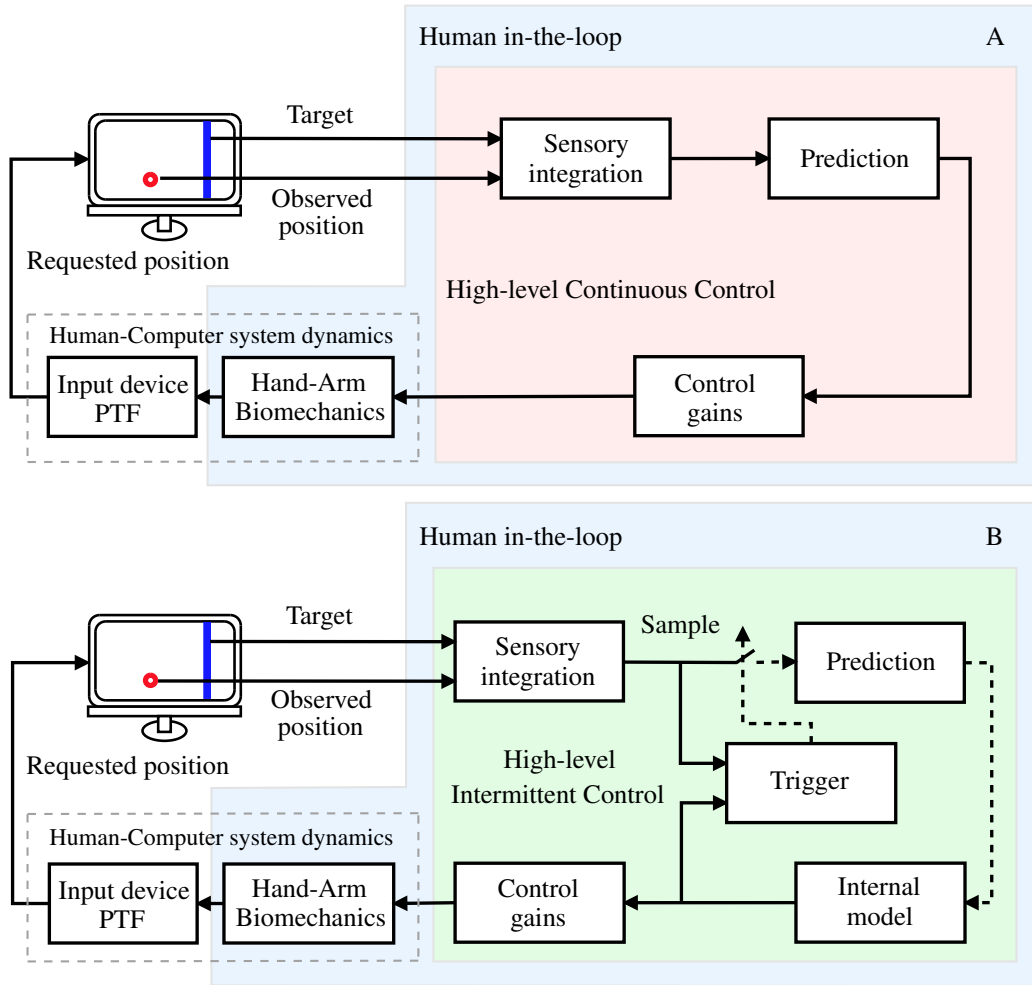


Figure 2: The continuous control (CC, above) and intermittent control (IC, below) frameworks in the context of a general HCI task. The black solid lines represent signals going in and out the different systems continuously, whereas the dashed lines indicate that they are active intermittently. (A) Continuous control performs three tasks: Sensory integration, Prediction, and input generation modulated by a set of Control gains. (B) Intermittent control (green box), includes an Internal reference model, a Trigger, and Sampling mechanism. Both models take into account the Human-Computer system dynamics (grey dashed-line box) as the combination of two separate systems: The Hand-Arm Biomechanics and the Input Device Pointing Transfer Function (PTF). The pointing task is to bring the displayed pointer (red circle) to the Target (blue vertical bar). The user is represented in blue.

The aforementioned process can be defined by three main components: 1) the system that describes the evolution in time (time-series) of the controlled variable or output, known simply as the *system*, which includes the computer hard-

and software, 2) a high-level controller in charge of sensing outputs, predicting future states and generating control inputs which is implemented in the users' CNS and finally, 3) the neuromuscular system (NMS) of the user which provides the necessary correction, normally as a force or torque applied to a pointing mechanism, such as a joystick or a computer mouse.

A continuous flow of signals between a system and its user through any given interface is an example of a continuous interaction model where the system output is continuously being sensed and consequently, control commands are generated as a result of this continuous stream. Although this continuous model has been the dominant framework to explain motor control, there are situations where this closed-loop system is not always continuous, for instance when the contact between the hand and the input device to the system is interrupted (Loram et al., 2011), or when the system output is not available for measurement. These situations yield a system that is intermittently-continuous. However, a third source of intermittent behaviour arises as a result of the refractory period that is observed frequently in reaction tasks (Telford, 1931), which implies that even with a continuous flow of information in the form of feedback, humans respond to a succession of sufficiently rapid stimuli in a serial way, starting the response for new stimuli only after finishing the processing and execution of the previous one, thus evolving for short periods of time in an open-loop configuration (Craik, 1947; Navas and Stark, 1968). This serial-ballistic operation mode is at the core of the intermittent control model that is presented in this paper for HCI tasks, providing a flexible architecture that includes continuous interaction as a special case of a more general framework.

3.1 The intermittent control framework

Let us introduce the general intermittent control model by presenting the continuous control counterpart first using a block diagram, which is a common graphical representation of the structure and purpose of a control system. In Fig. 2A (above), a continuous interaction model is shown in the context of target tracking using a pointer device (e.g., computer mouse or joystick). The arrows represent signals travelling through the loop that act as inputs and outputs to the different *systems* in the model (depicted as white boxes with solid black borders). The user is represented by the light blue coloured box containing two subsystems, the *Human-Computer system dynamics* box (in grey dashed lines) which includes the dynamics of the arm and hand in relationship to the pointer device, and a high-level continuous controller (CC) shown in a red coloured box comprised by three blocks: Sensory integration, Prediction, and Control gains. The *Human-Computer system dynamics* box contains the group of variables that the user attempts to control and it receives a correcting input signal that the CC system generates. The mouse velocity measured by the mouse sensor is transferred to the pointer velocity via a possibly non-linear pointing transfer function (PTF) (Casiez et al., 2008; Casiez and Roussel, 2011). The output of this block (e.g., pointer position on a display) is then sensed via visual feedback and used to generate a new control action. The CC system as a whole is in charge of reducing the error between the target signal (desired pointer position) and the output (current pointer position) by combining sensory streams and intended targets to form an internal model of the task at hand. It is argued that the brain uses some form of model based *Prediction* to better understand the consequences of our commands during movement and to diminish the effect of slow transmission pathways (Miall et al., 1993; Bhushan and Shadmehr, 1999; Gawthrop and Wang, 2008; Gawthrop et al., 2011), this concept is represented by the block that follows the system integration process. The last stage involves the selection and computation of an appropriate high-level *Control* signal which is applied continuously.

The IC model, shown in Fig. 2B (below), incorporates the same elements of the continuous control model with the addition of a *Trigger* mechanism within the user's CNS, that has the fundamental role of opening or closing the loop right after the output of the sensory integration process; this effectively *samples* the output and relevant states of the system. Regulating the flow of information at this point allows the user to achieve continuous measurement of the output variables while applying control commands intermittently. This mechanism can replicate refractoriness by enforcing a minimum amount of time in which the system would evolve in an open-loop configuration. In addition to this, the controller could extend these open-loop intervals beyond this minimum time by comparing the states of an internal dynamical model which represents the task and the sensory outputs coming in the form of feedback. This concept is discussed in the following section.

3.2 Event generation based on an internal model

The generation of control commands by the user in IC (shown in Fig. 2B) can be seen as the interplay of an *Internal model* and a set of *Control gains* within the CNS of the user that modulate the input signal that is applied to the system. The internal model is a central feature of IC and serves as reference in terms of performance, using a dynamical model to mimic the behaviour of a continuous delay-free version of the system (Gawthrop et al., 2015); therefore, in the ideal scenario of control inputs and system outputs that are not corrupted by motor or observation noise respectively, or affected by external *disturbances*, the states of this internal model should match the ones generated by the sensory integration process.

On the other hand, if the observations predicted by the user differ from the actual observations, it means that there are unaccounted disturbances which produce a deviation from the reference internal model. It is possible to use this source of error to decide if the sampling mechanism should stay open or to close it, which would update the Prediction stage and consequently the internal model itself with measured states. During the time in which the sampling mechanism is open, the internal model is evolving on its own and producing states *continuously* without using available feedback information, the fact that this process happens continuously ensures that a control signal is always going to be computed. In the case of a discrete movement, such as the initial ballistic submovement towards the target (surge), the motor signals in charge of the execution are planned in advance and executed ballistically. In order to plan such a ballistic movement, the internal model is necessary. One way to determine the mode in which the overall control loop should operate (open vs closed-loop) is to compare the error between the sensed output and the version of the output generated by the internal model against a fixed value, establishing a triggering *threshold*. If the error is larger than the threshold then the controller should rely on feedback to reduce it (trusting sensed information more). This constant comparison carried out by the trigger mechanism generates *events*, which define the moment in time when the error overcomes the threshold value. This particular implementation of IC is often referred as Event-Based or Event-Driven IC (Gawthrop and Wang, 2009). When an event is created, the feedback loop is closed only for a small instant and then reopened, which forces the controller to stay open-loop for a minimum amount of time before feedback can be used again due to new events.

The IC model shown in Fig. 2B was conceived from a computational perspective as an additional layer of an existing continuous model proposed by Kleinman, which used a linear optimal controller to approximate the response of a human operator in manual control tasks (Kleinman, 1969; Kleinman et al., 1970). The previously mentioned elements of sensory integration, prediction, and control generation formed the basis for Kleinman's model, linking physiology concepts with control theory, while providing solid basis for IC.

3.3 Human variability in motion

Variability is a distinctive element of human motion and human-in-the-loop systems. A human generating a control action repeatedly over a system with a defined set of external perturbations, would generate output responses that are slightly different from each other. Physiologically, variability is generated at any level of the motor pathway and it is normally attributed to a combination of factors: 1) neural spike initiation-propagation, as well as synaptic transmission and muscle activation, all rely on biophysical and chemical events which are stochastic in nature (Jones et al., 2002; de C. Hamilton et al., 2004; Faisal and Laughlin, 2007; Faisal et al., 2008) and, 2) variation in movement planning and decision making processes happening in the CNS (Dhawale et al., 2017; Gollee et al., 2017).

From a computational point of view, the variability of human movements has been explained by adding motor and observation noise to a continuous representation of the overall closed-loop system (Levison et al., 1969; Van Der Kooij and De Vlugt, 2007; Van Der Kooij and Peterka, 2011), implying that these differences are the result of a linear process in combination with a stochastic component, introduced by the random noise. However, there is experimental evidence that shows how manual control is subject to a refractory process (Navas and Stark, 1968; Miall, 1986; Loram et al., 2011, 2014), strengthening the view of sustained sensorimotor control as a discrete sequence of open-loop intervals combined with feedback instances of sensory information. It has also been proposed that a triggering mechanism is behind the decision of closing or opening the feedback loop, where the timing of each event is decided by error signals crossing a threshold value.

Results from a visuo-manual tracking task (Loram et al., 2011; Gollee et al., 2017), in which the participants used a joystick to control the position of an unstable dynamical system (represented by a dot on a screen), showed that an intermittent-predictive controller is able to explain both the linear and nonlinear components of the output response at both excited and non-excited frequencies, without adding any coloured noise. Whereas a continuous predictive controller requires the addition of a separate motor noise profile for each of the conditions in the experiment to adequately describe the output response. These findings suggest not only that the aperiodic triggering mechanism is a plausible hypothesis to explain manual tracking but also that the intermittency is directly related to the observed variability.

The constant switching between open and closed-loop evolution introduces other benefits, such as the possibility to clearly distinguish the effects of the applied input commands, the external disturbances and the natural dynamics of the system (Loram et al., 2011). Moreover, the variability that is introduced by the aperiodic triggering process of IC plays an important role in adaptation and learning by regulating the trade-off between exploration and exploitation (Loram et al., 2015). It has been shown that higher rates of movement-to-movement variability in motor output predict faster learning rates for specific motor control tasks. This suggests that regulating variability according to the environment and the task at hand might be an essential feature of the CNS to promote either fine control when precision is needed or broad exploration to accelerate adaptation and learning (Wu et al., 2014).

4 The intermittent control model

In this section, a more detailed explanation of IC is given, with an emphasis on describing the main elements of the framework more formally, from a control theory perspective, to support a reader wishing more insight into the model structures, rationale and behaviour. While the theory of IC in this section is fundamental to understand the details of the framework as a control methodology, the main results of the paper are largely accessible if skipped at a first reading. The high-level IC described in Fig. 2B in the context of a pointing task, is reintroduced using a more general approach in Fig. 3, which is in turn based on the versions presented in (Gawthrop and Wang, 2007; Gawthrop et al., 2011, 2015). Together, the *Hand-Arm Biomechanics* and *Input device PTF* blocks from Fig. 3 represent a mathematical model of the neuromuscular dynamics of the user and the user interface. Although user interface dynamics can, in principle, be highly nonlinear, e.g., via nonlinear PTFs, for simplicity in the following we assume that the overall dynamics can be expressed as a linear state-space model of order n , that corresponds to the case of constant gain in pointing, and which can be expressed as follows:

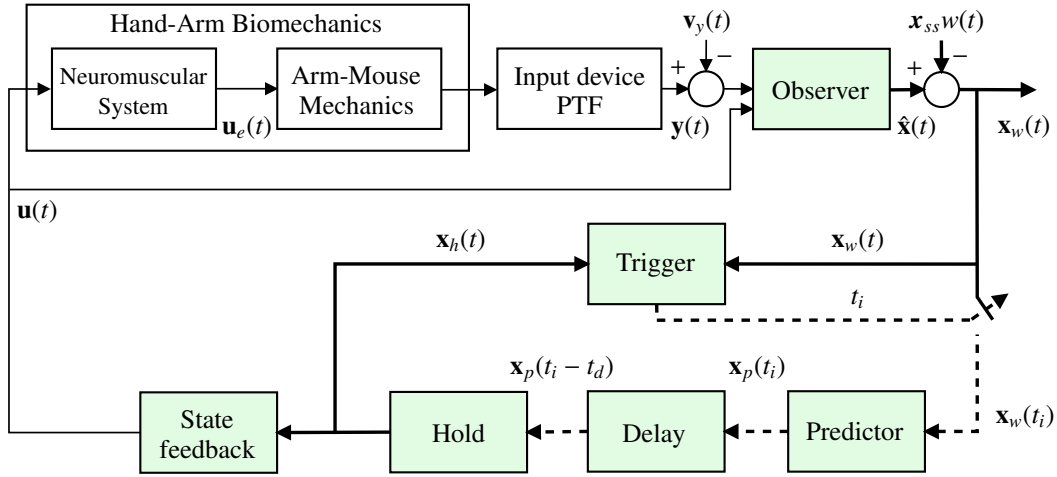


Figure 3: Diagram of the intermittent controller within the CNS of the user. The hold states \mathbf{x}_h are compared with the state-estimates \mathbf{x}_w in the trigger block. If the difference exceeds a predefined threshold, then the block creates events at times denoted by t_i . The hold states \mathbf{x}_h are used to generate the control signal \mathbf{u} during the open-loop period, and it is reset only at times t_i by the predictor block. The dashed lines represent signals that are defined only at t_i . The thick lines/arrows of the diagram represent vector signals, whereas the thin ones represent scalar versions, for the single-input single-output case. This figure is based on the representation given in (Gawthrop et al., 2011). The *Hand-Arm Biomechanics* block contains the *Neuromuscular System* which generates the force that is applied to the input device and the *Arm-Mouse Mechanics* block that translates it into input to the pointing transfer function.

$$\begin{aligned}\dot{\mathbf{x}}(t) &= \mathbf{A}\mathbf{x}(t) + \mathbf{B}\mathbf{u}(t) \\ \mathbf{y}(t) &= \mathbf{C}\mathbf{x}(t),\end{aligned}\tag{1}$$

with $\mathbf{x}(0) = \mathbf{x}_0$ as initial condition and where $\mathbf{x} \in \mathbb{R}^n$ corresponds to the system state such as pointer position and velocity, and muscle activation, $\mathbf{y} \in \mathbb{R}^{n_y}$ corresponds to the output such as pointer position on the display, and $\mathbf{u} \in \mathbb{R}^{n_u}$ corresponds to the input such as muscle excitation. t represents continuous time. \mathbf{A} is a $n \times n$ matrix representing how the system evolves without control input, \mathbf{B} is a $n \times n_u$ matrix, representing the impact of control signals such as muscle excitation on the system, and \mathbf{C} is a $n_y \times n$ matrix, representing how the system state maps to the users' observation, such as pointer position on the display.

Two concepts from control theory are potentially generally useful for HCI models. These are the *observer* and the *predictor*. The control goal of the user is to bring the system output $\mathbf{y}(t)$ as close as possible to the target signal $w(t)$ (e.g., the pointing target). The system integration process mentioned in Fig. 2B which combines multiple sensory channels, can be interpreted as an estimation problem. The central issue is that the control problem might not be solvable from the observations alone, if the true state is unknown. For example, in pointing, the user can observe only the pointer position. If the pointer velocity, muscle activation etc. can not be observed directly, they need to be estimated in order to enable the user to control the system.

Observer: To solve this issue, the input $\mathbf{u}(t)$ and the output $\mathbf{y}(t)$ are fed to a linear *observer*, which is a dynamical model based on (1), that reconstructs the full state of the system $\hat{\mathbf{x}}(t)$ using only output measurements and information

on the input that is being applied. Once the target signal $w(t)$ has been introduced as $\mathbf{x}_w(t) = \hat{\mathbf{x}}(t) - \mathbf{x}_{ss}w(t)$, the resulting observed states $\mathbf{x}_w(t)$ get sampled, this updates the rest of the structures in the feedback loop, only at discrete points in time t_i .

Predictor: In this implementation, the role of the *predictor* is to compensate for transmission time-delays which might be present in the feedback loop both from the users neural system and from the computer system, this is done by predicting the future states of the system $\mathbf{x}_p(t_i)$ based on the state estimates $\mathbf{x}_w(t_i)$ which are defined only when a sample is taken.

The concept of an internal model mentioned earlier in Fig. 2B, is represented in control terms as a generalised *hold*, which is a dynamical model that mimics the behaviour of the overall closed-loop system by continuously generating the state vector $\mathbf{x}_h(t)$. The *trigger* compares the hold states $\mathbf{x}_h(t)$ and the observed states $\mathbf{x}_w(t)$ to generate a prediction error e_p . An event is generated by the trigger at t_i once e_p exceeds a predefined threshold q . The hold states $\mathbf{x}_h(t)$ are used to compute a *state feedback* control input $\mathbf{u}(t)$ continuously, which is the signal that drives the neuromuscular system producing the final input to the system $\mathbf{u}_e(t)$. Notice that both the input $\mathbf{u}(t)$ and the output $\mathbf{y}(t)$ can be affected by motor noise $\mathbf{v}_u(t)$ and sensory noise $\mathbf{v}_y(t)$ respectively.

Before introducing definitions for the hold, the predictor and the trigger mechanism, it is important to define the different time frames that are used in IC to accurately distinguish between what happens during the open-loop intervals and the instances of feedback.

4.1 Intermittent control time-frames

IC combines the use of the following time-frames:

1. **Continuous-time** (t), represents the time in which the system defined in equation (1) evolves.
2. **Discrete-time** (t_i), time instants at which an event is generated, indexed by i . The time between event instants is known as the *intermittent interval* Δ_i . The i th intermittent interval can be defined as

$$\Delta_{ol} = \Delta_i = t_{i+1} - t_i. \quad (2)$$

A *sampling delay* Δ_s can be used to sample the observed states $\mathbf{x}_w(t)$ once a fixed-time interval has elapsed after the detection of an event at t_i . If $\Delta_s = 0$ then the sample is taken at t_i .

3. **Intermittent-time** (τ), a continuous variable that is restarted every Δ_i according to

$$\tau = t - t_i. \quad (3)$$

A lower limit Δ_{ol}^{\min} can be specified within a given intermittent interval as

$$\Delta_i > \Delta_{ol}^{\min} > 0. \quad (4)$$

The lower limit Δ_{ol}^{\min} , also known as *minimum open-loop interval*, has been used before to model the *psychological refractory period* observed in human motor control (Gawthrop et al., 2011).

Based on these definitions, it is now possible to define the model used as the generalised hold, which is a continuous closed-loop approximation of the overall system that relies on the following underlying controller.

4.2 Underlying continuous controller

A state-feedback controller for the system in equation (1), with gain \mathbf{k} , can be established by implementing the following control-law

$$\mathbf{u}(t) = -\mathbf{k}\mathbf{x}(t). \quad (5)$$

Standard procedures such as pole-placement or the linear quadratic regulator (LQR) approach (Goodwin et al., 2001) can be used to obtain the gain \mathbf{k} . The resulting closed-loop system, defined by the state vector \mathbf{x}_c is

$$\dot{\mathbf{x}}_c(t) = \mathbf{A}_c\mathbf{x}_c(t), \quad (6)$$

which depends on $\mathbf{x}_c(0) = \mathbf{x}_0$ as the initial condition and a closed-loop matrix \mathbf{A}_c defined as follows

$$\mathbf{A}_c = \mathbf{A} - \mathbf{B}\mathbf{k}. \quad (7)$$

The target signal $w(t)$ can be introduced by defining the following system

$$\begin{aligned} \mathbf{0}_{n \times 1} &= \mathbf{A}\mathbf{x}_{ss}(t) + \mathbf{B}\mathbf{u}_{ss}(t) \\ \mathbf{y}_{ss}(t) &= \mathbf{C}\mathbf{x}_{ss}(t), \end{aligned} \quad (8)$$

where \mathbf{x}_{ss} , \mathbf{u}_{ss} , and \mathbf{y}_{ss} correspond to the steady-state versions of the states, inputs, and outputs respectively. Solving for \mathbf{x}_{ss} and \mathbf{u}_{ss} can be done by writing the system as follows

$$\begin{bmatrix} \mathbf{x}_{ss}(t) \\ \mathbf{u}_{ss}(t) \end{bmatrix} = \begin{bmatrix} \mathbf{A} & \mathbf{B} \\ \mathbf{C} & \mathbf{0} \end{bmatrix}^{-1} \begin{bmatrix} \mathbf{0}_{n \times 1} \\ 1 \end{bmatrix}. \quad (9)$$

Thus, the overall control input from (5) can be redefined as

$$\begin{aligned} \mathbf{u}(t) &= -\mathbf{k}(\mathbf{x}(t) - \mathbf{x}_{ss}w(t)) + \mathbf{u}_{ss}w(t) \\ &= -\mathbf{k}\mathbf{x}(t) + (\mathbf{u}_{ss} + \mathbf{k}\mathbf{x}_{ss})w(t). \end{aligned} \quad (10)$$

By defining $\mathbf{r} = \mathbf{u}_{ss} + \mathbf{k}\mathbf{x}_{ss}$, a simplified expression is obtained

$$\mathbf{u}(t) = -\mathbf{k}\mathbf{x}(t) + \mathbf{r}w(t). \quad (11)$$

The expression in (11) reduces the error between the output $\mathbf{y}(t)$ and the target signal $w(t)$, depending on the value of the gain \mathbf{k} . This assumes that the matrices \mathbf{A} and \mathbf{B} are such that the model in (1) is *controllable* with respect to $\mathbf{u}(t)$, which means that the control input $\mathbf{u}(t)$ has the ability to drive the state-vector $\mathbf{x}(t)$ from its initial condition to any final value in a finite amount of time.

4.3 State observer

In many cases, the system state $\mathbf{x}(t)$ in (1) is not fully available for direct measurement. For example, usually only the pointer position is shown by the computer, but not the pointer velocity. One way to overcome this is to implement a state observer that estimates the portion of $\mathbf{x}(t)$ that is not known using only available information such as the output $\mathbf{y}(t)$, known states, and the current input $\mathbf{u}(t)$. An observer for the system described in (1) can be designed by defining a vector $\hat{\mathbf{y}}(t)$ which contains all the available signals as follows

$$\dot{\hat{\mathbf{x}}}(t) = \hat{\mathbf{A}}\hat{\mathbf{x}}(t) + \mathbf{B}\mathbf{u}(t) + \mathbf{L}[\hat{\mathbf{y}}(t) - \mathbf{v}_y(t)] \quad (12)$$

where $\hat{\mathbf{A}} = \mathbf{A} - \mathbf{L}\hat{\mathbf{C}}$ and $\hat{\mathbf{y}}(t)$ is defined as

$$\hat{\mathbf{y}}(t) = \hat{\mathbf{C}}\mathbf{x}(t). \quad (13)$$

Therefore, the matrix $\hat{\mathbf{C}}$ defines which elements from $\mathbf{x}(t)$ are used as inputs for the observer in order to reconstruct the full state. The matrix \mathbf{L} is a design parameter similar to the feedback gain \mathbf{k} in that both of them can be designed via pole-placement or LQR methods.

4.4 Generalised hold

The generalised hold uses the dynamics imposed by (7) to define the open-loop behaviour in IC. This is achieved by implementing the following state-feedback control-law

$$\mathbf{u}(t) = \mathbf{u}(t_i + \tau) = -\mathbf{k}\mathbf{x}_h(\tau), \quad (14)$$

where the hold states \mathbf{x}_h evolve in the intermittent time τ according to the following autonomous system

$$\dot{\mathbf{x}}_h(\tau) = \mathbf{A}_h\mathbf{x}_h(\tau). \quad (15)$$

When the observed states are sampled at $t = t_i$, the hold states \mathbf{x}_h are reinitialised using vector \mathbf{U}_i as follows

$$\mathbf{U}_i = \mathbf{K}_h\mathbf{x}_p(t_i - t_d). \quad (16)$$

Expression (16) takes the predicted states $\mathbf{x}_p(t_i - t_d)$, which cancel the effect of the time-delay t_d , to reset the hold state \mathbf{x}_h at the start of each intermittent interval

$$\mathbf{x}_h(t_i) = \mathbf{U}_i. \quad (17)$$

The square matrix $\mathbf{K}_h = \mathbf{I}_{n \times n}$ in (16) is defined as the *intermittent control gain*. The overall dynamics of the autonomous system in (15) are then determined by matrix \mathbf{A}_h . If the closed-loop matrix \mathbf{A}_c in (7) is used as follows

$$\mathbf{A}_h = \mathbf{A}_c, \quad (18)$$

then the generalised hold becomes a *system-matched hold* (Gawthrop and Wang, 2011), that effectively approximates the dynamics of the closed-loop system defined in (6). The assignment in (18) provides a common ground to compare the estimated states provided by the observer and to those coming from the hold, which can be seen as reference states for the IC framework.

4.5 Intermittent prediction

A predictor can be implemented as a compensation strategy in the presence of time-delays. The following dynamical system can be established during the intermittent time frame τ

$$\dot{\mathbf{x}}_p(\tau) = \mathbf{A}\mathbf{x}_p(\tau) + \mathbf{B}\mathbf{u}(\tau), \quad (19)$$

with $\mathbf{x}_p(0) = \mathbf{x}_w(t_i)$ and evaluated at $\tau = t_d$. Combining (19) and (15) yields the following extended system

$$\frac{d}{d\tau}\mathbf{X}(\tau) = \mathbf{A}_{ph}\mathbf{X}(\tau), \quad (20)$$

subject to $\mathbf{X}(0) = \mathbf{X}_i$ as the initial condition, and where

$$\mathbf{A}_{ph} = \begin{bmatrix} \mathbf{A} & -\mathbf{B}\mathbf{k} \\ 0_{n \times n} & \mathbf{A}_h \end{bmatrix}. \quad (21)$$

The extended state vector \mathbf{X} from (20) is defined as $\mathbf{X}(\tau) = \begin{bmatrix} \mathbf{x}_p(\tau) & \mathbf{x}_h(\tau) \end{bmatrix}^T$ during the open-loop interval. At t_i , \mathbf{X} takes the following form

$$\mathbf{X}_i = \begin{bmatrix} \mathbf{x}_w(t_i) \\ \mathbf{x}_p(t_i - t_d) \end{bmatrix}. \quad (22)$$

The solution of (19) at $\tau = t_d$ yields

$$\mathbf{X}(t_d) = e^{\mathbf{A}_{ph}t_d}\mathbf{X}_i. \quad (23)$$

From (23), the predicted states \mathbf{x}_p can be obtained every intermittent interval using the following expression

$$\mathbf{x}_p(t_i) = \mathbf{E}_{pp}\mathbf{x}_w(t_i) + \mathbf{E}_{ph}\mathbf{x}_h(t_i), \quad (24)$$

where the matrices \mathbf{E}_{pp} and \mathbf{E}_{ph} of dimension $n \times n$, are partitions of the $2n \times 2n$ matrix \mathbf{E} defined as

$$\mathbf{E} = e^{\mathbf{A}_{ph}t_d} = \begin{bmatrix} \mathbf{E}_{pp} & \mathbf{E}_{ph} \\ \mathbf{E}_{hp} & \mathbf{E}_{hh} \end{bmatrix}. \quad (25)$$

Both \mathbf{E}_{pp} and \mathbf{E}_{ph} can be obtained offline.

4.6 Event detection

IC produces an aperiodic sequence of events, determined by the error between the hold states \mathbf{x}_h and the closed-loop observer state \mathbf{x}_w as follows

$$e_x = \mathbf{x}_h(t) - \mathbf{x}_w(t). \quad (26)$$

An event is generated when e_x is greater than a predefined threshold q , according to the following quadratic switching function

$$e_x^T(t) \mathbf{Q}_t e_x(t) > 1, \quad (27)$$

where \mathbf{Q}_t is a positive semi-definite matrix that defines which states are considered in order to detect events and thus trigger the use of feedback. For instance, an IC triggering on the error of a two dimensional state vector would implement the next switching function

$$\left(\frac{e_{x_1}}{q_1}\right)^2 + \left(\frac{e_{x_2}}{q_2}\right)^2 > 1, \quad (28)$$

with a matrix \mathbf{Q}_t containing the following values in its diagonal

$$\mathbf{Q}_t = \begin{bmatrix} \frac{1}{(q_1)^2} & 0 \\ 0 & \frac{1}{(q_2)^2} \end{bmatrix}. \quad (29)$$

This particular choice of the event detection mechanism allows to set different threshold values for specific states and to use different combinations of them.

5 Experiment Setup and Dataset

The results shown in this paper are based on the *Pointing Dynamics Dataset* that was collected from a mouse pointing experiment described in (Müller et al., 2017). The IC framework from the previous sections is used to identify the parameters of a standard intermittent controller. The full dataset is publicly available.⁴ In the aforementioned experiment, 12 participants were asked to control a white pointer that was shown on a screen. The pointer reflected the changes in the x -dimension of the mouse exclusively and it was restricted to move only horizontally.

The task consisted of clicking a number of one-dimensional targets that were displayed in sequence. During a block of trials, the active target was presented in a different color compared to the previous target, and the distance between them, as well as the width of the target, stayed constant throughout the block. Each block uses a specific combination of distance and width; a total of 8 combinations were applied for each subject: 1) distance of 212 mm and widths of 0.83, 3.32, 14.1 and 70.6 mm, 2) distance of 353 mm and widths of 1.38, 5.54, 23.5, 118 mm. Fitts' law (Fitts, 1954) states that the time required to move to a specific target area MT is a function of both the distance to the target D and the size of the target W as follows

$$MT = a + bID, \quad (30)$$

where the Index of Difficulty (ID) is

$$ID = \log_2 \left(\frac{D}{W} + 1 \right), \quad (31)$$

which is known as the Shannon formulation (MacKenzie, 1992). Based on (31) and the selected combinations of distance between targets and target width, the resulting ID for both 212 mm and 353 mm conditions are 8, 6, 4 and 2. Therefore, each participant had to complete a full block of trials per ID for the two distance conditions. The experiment blocks were designed to have 102 trials each, divided into 22 trials for training and 80 for the rest of the task.

The participants were asked to stay below a 5% error rate while clicking on every target as quickly as possible. A beep sound would indicate the user if the click was made outside the target area, triggering the appearance of the next target on screen for that particular block. The users were not asked to repeat failed trials (missed targets). All participants completed a training phase of 22 trials for each block before starting the experiment and had a short break between to rest between blocks.

6 Model implementation and controller design

The intermittent controller shown in Fig. 3 was implemented in Matlab⁵ using the Control Systems Toolbox to generate appropriate transfer function and state-space representations of the human dynamics and the system to be controlled. The block labelled as *Neuromuscular system* in Fig. 3 was implemented as a second order system with time-constants of 50 ms (Milner-Brown et al., 1973),

$$G_{nms}(s) = \frac{1}{(0.05s + 1)^2}, \quad (32)$$

where $G(s)$ is the transfer function in the Laplace domain. This transfer function was converted to its equivalent state-space system in the form of equation (1) with

$$\mathbf{A}_{nms} = \begin{bmatrix} -20 & 20 \\ 0 & -20 \end{bmatrix}, \quad \mathbf{B}_{nms} = \begin{bmatrix} 0 \\ 20 \end{bmatrix}, \quad \mathbf{C}_{nms} = \begin{bmatrix} 1 & 0 \end{bmatrix}. \quad (33)$$

Similarly, the block shown in Fig. 3 as *Arm-Mouse Mechanics* was established as a double integrator in the state-space representation of (1) with

$$\mathbf{A}_{sys} = \begin{bmatrix} 0 & 1 \\ 0 & 0 \end{bmatrix}, \quad \mathbf{B}_{sys} = \begin{bmatrix} 0 \\ 1 \end{bmatrix}, \quad \mathbf{C}_{sys} = \begin{bmatrix} 1 & 0 \end{bmatrix}, \quad (34)$$

where the associated state vector is $\mathbf{x}_{sys}(t) = \begin{bmatrix} \mathbf{x}_{pos}(t) & \mathbf{x}_{vel}(t) \end{bmatrix}^T$, comprised of the pointer position $\mathbf{x}_{pos}(t)$ and velocity $\mathbf{x}_{vel}(t)$. This assumes that the output of the neuromuscular system, depicted as $\mathbf{u}_e(t)$ in Fig. 3, is a force generated by the participant, applied to a unit mass in a low friction environment, and that the output of the overall system, $\mathbf{y}(t)$, is the position of the mass, which in this case is equivalent to the position of the pointer on the screen. The combination of (33) and (34) yields a fourth order system based on the full state vector $\mathbf{x}(t)$, which is then used to design the overall controller.

⁴<http://joergmueller.info/controlpointing/>

⁵Matlab release version R2019a. The MathWorks, Inc., Natick, Massachusetts, United States.

The feedback gain vector \mathbf{k} shown in (5) was designed using optimal control via the LQR design method (Goodwin et al., 2001), to ensure that the closed-loop matrix \mathbf{A}_c , which defines the behaviour of the generalised hold in IC (18), has stable eigenvalues. This involves the minimisation of the LQR cost function

$$J_{LQR} = \int_0^{\infty} [\mathbf{x}(t)^T \mathbf{Q}_c \mathbf{x}(t) + \mathbf{u}(t)^T \mathbf{R}_c \mathbf{u}(t)] dt, \quad (35)$$

and the solution of its associated algebraic Riccati equation. Both $\mathbf{x}(t)$ and $\mathbf{u}(t)$ in (35) are weighted by design matrices \mathbf{Q}_c (an $n \times n$ diagonal matrix that must be positive semi-definite) and \mathbf{R}_c (an $n_u \times n_u$ diagonal positive definite matrix, where n_u corresponds to the number of inputs in the system). The diagonal nature of \mathbf{Q}_c is in fact a design choice, which is based on the assumption of not having crossed-term effects between the states. Using the same LQR method on the dual problem of state estimation, the closed-loop observer gain matrix \mathbf{L} , can be computed to force the estimation error to vanish asymptotically, by choosing a design matrix \mathbf{Q}_o . The observation matrix in (13) was defined as $\hat{\mathbf{C}} = \begin{bmatrix} 1 & 0 & 0 & 0 \end{bmatrix}$, which means that only the first state of the state vector $\mathbf{x}(t)$, corresponding to the pointer position $\mathbf{x}_{pos}(t)$, is used by the observer to estimate the rest to the unknown states. In the context of this work, matrices \mathbf{Q}_c and \mathbf{Q}_o were defined as parameters to be optimised, whereas \mathbf{R}_c was fixed for the entire process with a value of 1 (in this case it is a scalar since there is only one input to the system, $n_u = 1$). The time-delay t_d remained constant at 0.01 sec for all participants and conditions. Note that the effective time-delay is a combination of the constant t_d and the optimised threshold q and minimum open-loop interval Δ_{ol}^{\min} .

To detect events, a threshold q was applied only to $\mathbf{x}_{pos}(t)$. However, the actual value of q was obtained via the optimisation process. As suggested in (Gawthrop and Wang, 2009), the use of a *disturbance observer* is recommended to reduce the effect of zero mean constant disturbances $\mathbf{d}(t)$ at the input; therefore, an integrator is normally used to account for them and compensate accordingly.

7 Optimisation approach

Based on the systems (33) and (34), an optimisation procedure was used to fit a set of controller parameters to the experimental data. The following parameters were identified as a result of the optimisation process: The LQR design matrices \mathbf{Q}_c and \mathbf{Q}_o , the prediction error threshold q for triggering purposes, the minimum open-loop interval Δ_{ol}^{\min} and a mismatch gain $\mathbf{A}_p = 1 - p$.

The purpose of \mathbf{A}_p is to model the cases where the control input that is applied to system is different by a fixed amount from what it should be by design. This is implemented as follows: from Fig. 3, the output of the neuromuscular system $\mathbf{u}_e(t)$, which serves as the input to the system in (34), is multiplied by a quantity p , resulting in

$$\dot{\mathbf{x}}_{sys}(t) = \mathbf{A}_{sys} \mathbf{x}_{sys}(t) + \mathbf{B}_{sys} \mathbf{u}_{sys}(t), \quad (36)$$

where $\mathbf{u}_{sys}(t) = p \mathbf{u}_e(t)$. When $p = 1$, the full input is applied. A mismatch is generated when p is different than 1. The optimisation process identified the value of p directly; however, the mismatch gain \mathbf{A}_p is reported in the following sections as it gives a better insight on the difference between $\mathbf{u}_e(t)$ and $\mathbf{u}_{sys}(t)$. This discrepancy has a significant effect in the overall performance, specially when the states get close to the target position.

As observed in (Müller et al., 2017), the initial set of parameters used to start the optimisation process had a negligible effect on the resulting optimised parameters, converging consistently to the same set. As a consequence, a common starting point was selected for all conditions and subjects, which is shown in Table 1 including the lower and upper limits for each of them.

A pattern-search method was used for all subjects and conditions as implemented in Matlab's Optimisation Toolbox. Pattern-search methods are numerical optimisation routines that avoid the calculation or approximation of derivatives to minimise an objective function (Torczon, 1997). Based on a starting point, the method tries to find a new point that has a lower objective function value. The selection of the points to test is done based on pattern vectors which define points around the initial guess. If a lower objective function value is obtained for a particular point, then the point gets selected and a new set of scaled pattern vectors are applied (increasing the effective search area). If there is no point with a lower objective function value, then the area covered by the pattern vectors is reduced by a predefined factor. The process is repeated until a minimum is found. In general, these methods are useful to speed up repetitive optimisation tasks.

7.1 Data partitioning

The amount of data used for each optimisation differs from (Müller et al., 2017). Instead of fitting an intermittent controller to the entire block of trials, the data was partitioned according to the following criteria: the time elapsed

Table 1: Initial optimisation values*

	Parameter	Initial value	Min. value	Max. value	Units
LQR	\mathbf{Q}_o	10	0.00001	100000	-
	$\mathbf{Q}_{c,diag}$	$\begin{bmatrix} 1 & 1 & 1 & 1 \end{bmatrix}$	0.00001	100000	-
Timing	q	0.03	0.001	1	-
	Δ_{ol}^{min}	0.05	0.03	1	sec
Mismatch	p	0.9	0.1	2	-

* The values are shown in three different categories: \mathbf{Q}_c and \mathbf{Q}_o correspond to the LQR design parameters, the threshold q and the minimum open-loop interval Δ_{ol}^{min} as timing parameters, and finally the value of p which determines the mismatch gain $\mathbf{A}_p = 1 - p$. The minimum and maximum values for each parameter used as limits during the optimisation process are also shown.

between two successive changes in the target position would constitute a full *slice*. Essentially, each slice is composed of the pointer trajectories made by the subject to reach consecutive targets (two consecutive trials). An individual IC is then fitted to each slice. In Fig. 4, a prototypical target signal is used to illustrate how the data was partitioned into individual slices. Each block had 80 trials, this resulted in 40 full slices per block. The optimisation was carried out using the information of the last 20 slices in the block, leaving the rest for evaluation.

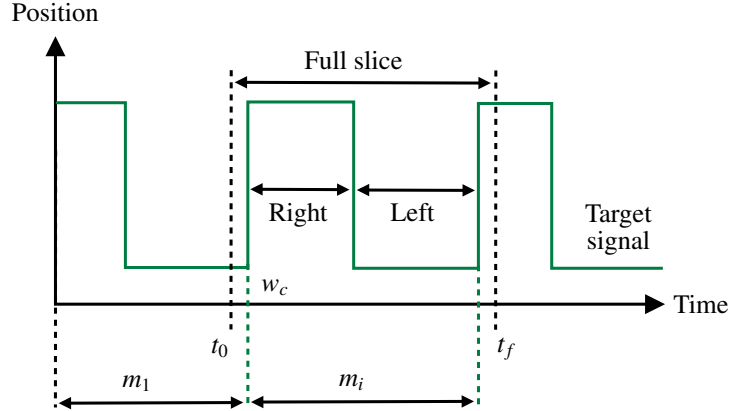


Figure 4: Data partitioning diagram. The figure shows a hypothetical target signal $w(t)$ (in green) to illustrate how the slices were delimited. The initial point of the slice t_0 starts 10 samples before a change in reference w_c where the participant has to move the pointer position to the target on the right side of the screen. The ending point t_f is 10 samples after the next change in reference in the same direction. The second portion of the slice (shown as *Left*) corresponds to the movement from the target on the right to the target on the left. As described in section 7.3, m_1 represents the best controller of the bank m , which is used to start a simulation and m_i is a randomly selected controller from the same bank.

7.2 Criteria for model fitness via cost functions

To establish how well the intermittent controller fits the experimental data, we use a general cost function J measuring the difference between pointer movement predicted by the model and actual pointer movement, which also includes the difference in terms of the pointer velocity. The optimiser considers the root mean squared error (RMSE) of these quantities as follows

$$J = c_p \sqrt{\frac{\sum_{i=1}^{n_j} (\hat{y}_i - y_i)^2}{n_j}} + c_v \sqrt{\frac{\sum_{i=1}^{n_j} (\hat{v}_i - v_i)^2}{n_j}}, \quad (37)$$

where \hat{y} and \hat{v} are the simulated pointer position and velocity respectively. The number of samples considered for each slice is shown as n_j and the constants c_p and c_v denote values that act as weights for each of the errors. The errors in (37) between the positions and velocities are squared, the result is averaged over the number of samples in each trial and then the square root of the obtained quantity is computed. This formulation provides a clear basis to evaluate the

fitness of the resulting intermittent controllers. For the optimisation procedure, the values of c_p and c_v were set to 0.5, resulting in equal weights for each of the error terms in (37).

7.3 Controller switching

The resulting models of the optimisation procedure can be used to carry out a simulation over a collection of trials for each participant. This can be done by selecting the best model available according to different criteria; for instance, selecting the model with the lowest RMSE score or the one that produced the lowest value of the cost function defined in (37). A simulation using this criterion would yield a response that is acceptable in terms of accuracy and steady-state error; however, it would not be able to capture some of the inherent variability of human control. To create a controller that exhibits an appropriately wide variety of responses, we took a multiple-model approach, instead of just applying a single model for all trials. This collection of parameters which are compatible with individual realisations of the behaviour helps represent the behavioural variability.

For all participants, a bank of models, which we will call m , was generated for each of the conditions in the experiment. This bank is essentially a ranked list based on the value of (37), that contains the intermittent controllers that were derived using the optimised parameters for each slice. This amounts to 20 controllers per condition. To start a simulation using this multiple model approach, the best controller in the bank, or m_1 , is used against the first trial, which is comprised from an initial pointer movement towards the right target followed by a second movement to the left target. This is illustrated in Fig. 4, where w_c shows the moment in time when the target changes. At w_c , a new controller m_i is selected from the model bank and applied for the duration of the next trial only, where i represents a random integer number between 1 and 20. This random selection of controllers from the bank m starts only after the first trial has finished and it is maintained until all the trials are completed. This effectively ensures that different controllers are used for a pair of back and forth movements, producing a trial response that is slightly different compared to the previous trial, resulting in a more variable trajectory overall.

The following section introduces the results obtained when this multiple-model approach is used to generate dynamic responses in order to compare them to the experimental data.

8 Modelling Results

The results obtained from the optimisation process applied to all participants and conditions are presented in this section. First, a visualisation of the observed variability in some of the responses is introduced, then the optimisation parameters obtained in each condition are shown including some of the dynamic responses showing the pointer position evolution, phase planes where position and velocity are compared, and Hooke plots which show the acceleration profiles through time.

8.1 Response variability

The ID of the task has a significant impact on the overall behaviour. In Fig. 5, the phase planes (pointer velocity in the vertical axis vs pointer position in the horizontal axis) for participants 1, 2 and 3 are shown to illustrate how the ID influences the control strategy and the human response. The bottom row (D, E, F), shows the experimental data for an ID of 8, which is regarded as the most difficult task in the experiment. A clear indicator of this is how small the target width is (0.83 mm), compared to a target width of 70.6 mm (ID of 2) presented in A, B and C. The target width is delimited by vertical lines on each side. For each condition, the experimental phase planes are shown in blue, whereas the ones in red correspond to the continuous second order lag controller (2ol) described in (Müller et al., 2017). The 2ol controller is different in many levels when compared to IC, but its most fundamental difference is the fact that it uses feedback at all times to generate the control input that is applied to the system.

The bottom row in Fig. 5 (D, E, F), shows responses where an initial burst in speed and position is made, commonly known as the surge, followed by a series of small position corrections as the pointer approaches the target. It is clear for instance that the landing position for the surge movement differs in every trial – a consequence of human variability. The top row of figures (A, B, C) exhibits a drastically different behaviour since the target width is greater, there is variability present but the participants seem to engage in an almost constant motion towards the targets without making corrections as they approach. The 2ol controller does a relatively good job tracking the easy conditions (ID 2); however, when applied to the most difficult condition (ID 8), the phase plane does not show the same level of variability seen in the experimental data. The parameters of the 2ol controller were also obtained via optimisation as described in (Müller et al., 2017) resulting in an individual parameter set for each condition, which was subsequently applied in simulation.

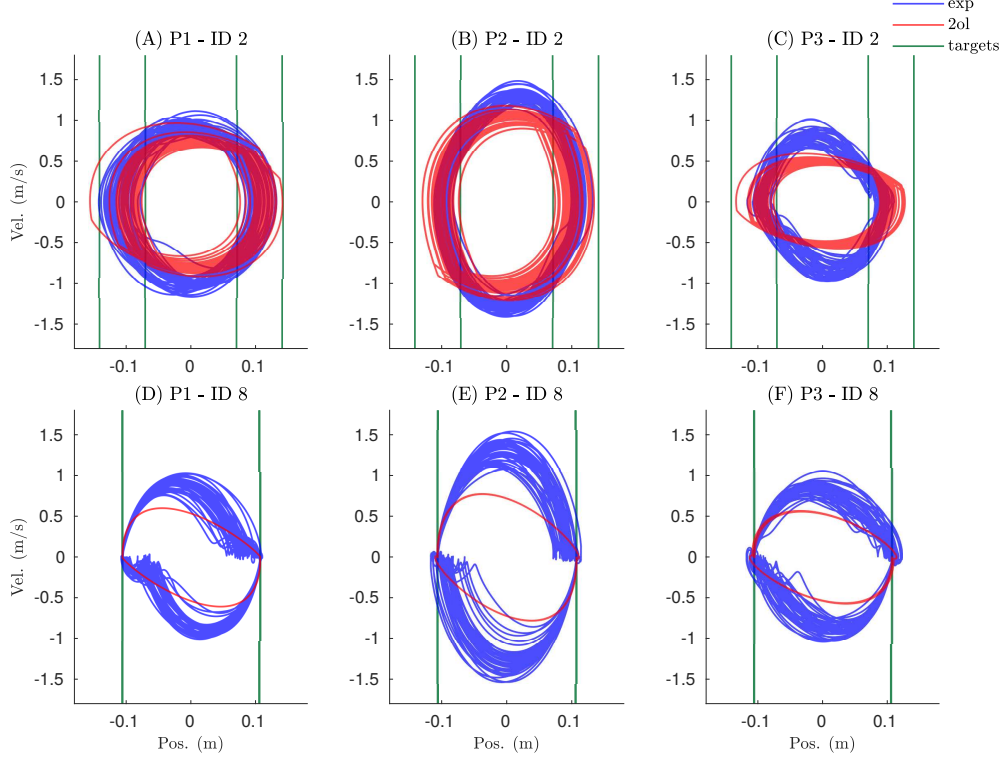


Figure 5: Phase planes showing pointer position vs. velocity for participants 1, 2 and 3. Experimental trajectories for each participant are shown in blue, left and right target limits are represented by green vertical lines, and the trajectories in red correspond to the second order lag model (2ol) from (Müller et al., 2017). A, B, and C, show data for a distance of 212 mm with a target width of 70.6 mm, corresponding to an ID of 2. D, E, and F, show data for the same distance between targets but with a different target width of 0.83 mm (ID 8). Participants 1, 2 and 3 are represented by each of the columns from left to right. From the simulated trajectories in red, it is clear that the 2ol model provides some degree of variability for ID 2 but when the ID increases, it does not reproduce the observed variability of the experimental trajectories.

8.2 Optimised parameters and their interpretation

The optimisation process had 4 free scalar parameters \mathbf{Q}_o , \mathbf{A}_p , q and Δ_{ol}^{\min} , as well as the matrix \mathbf{Q}_c , where only its diagonal elements are of interest (the off diagonal entries are zero), thus adding 4 extra parameters for a total of 8. In Fig. 6, the optimised parameters for all subjects are shown when grouped by ID. This includes the threshold q (A), the gain \mathbf{A}_p (B), the minimum open-loop interval Δ_{ol}^{\min} (C) and finally the observer gain \mathbf{Q}_o (D, shown in log scale). For each parameter, the data distribution is shown as a violin plot for the two different distances of 212 mm (left side) and 353 mm (right side) respectively, and grouped according to the ID.

Fig. 6A, shows that the threshold q has slightly larger values for ID 2, which is consistent for the distributions of both distances. The data are more concentrated for the cases of ID 4, 6, and 8 as shown by the narrow distributions. All conditions exhibit long tails, indicating the presence of higher thresholds in some of the optimised models. The mismatch gain \mathbf{A}_p in Fig. 6B also exhibits a clear trend. For ID 4, 6, and 8, the data distribution is wider for these three cases, indicating that there was less of a mismatch compared to ID2, which shows most of its values around $\mathbf{A}_p = 0.1$. The minimum open-loop interval Δ_{ol}^{\min} in Fig. 6C is comparable for the different levels of ID, showing that most of the data lie within a 0.03 to 0.05 sec range.

The values for the design matrix \mathbf{Q}_c are presented in Fig. 7 using a log scale, where 7A, B, C and D show the data of the four elements in the diagonal of matrix \mathbf{Q}_c . The first and second elements of \mathbf{Q}_c shown in Fig. 7A and Fig. 7B are of particular importance: \mathbf{Q}_{c1} , since it is associated to the position state which is the defined output of the controller, and \mathbf{Q}_{c2} is related to the pointer velocity state. These two values have a distinct impact in the overall transient behaviour. \mathbf{Q}_{c1} shows higher values across all conditions compared to the other elements in \mathbf{Q}_c , which means that the controller is trying to put more emphasis on the position state in order to reduce the error with respect to the reference. However, comparing the distributions for each ID in Fig. 7A, it can be seen that the optimisation yields controllers with higher

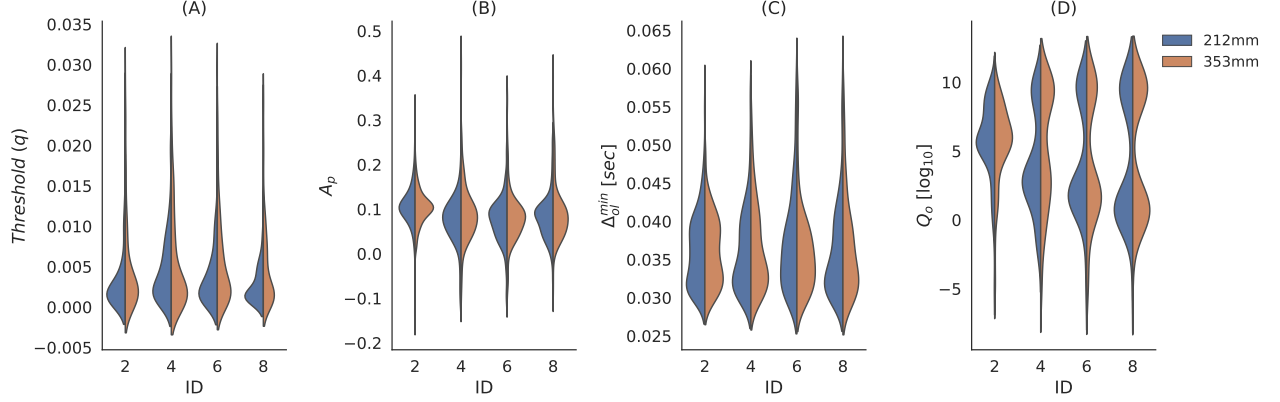


Figure 6: Optimised controller parameters for each condition. (A) the threshold q , (B) mismatch gain A_p , (C) the minimum open-loop interval Δ_{ol}^{min} , and (D) the observer gain Q_o are shown as violin plots including data of all subjects and categorised by ID (horizontal axis). The results are also grouped according to the two values of distance between targets used in the experiment (left: 212 mm and right: 353 mm). The shape of the distributions for ID 2 is slightly different compared to the rest of the conditions.

values of Q_{c1} for ID 2 in general, whereas the rest of the IDs have distributions that are similar in shape. This seems to be related to the result shown in Fig. 6B where ID 2 exhibits a larger model mismatch A_p . A plausible explanation is that the LQR method tries to compensate for the mismatch by assigning a higher weight on the position state, which in the end results in a higher controller gain. For Q_{c2} in Fig. 7B, the distributions are bimodal for all ID showing lower values in general compared to Q_{c1} . Similarly, the distribution of ID 2 presents more data grouped towards the positive range of values, indicating that the optimisation procedure penalised the velocity state more heavily. This is also in agreement with the result for A_p in Fig. 6B. Overall, the difference in behaviour of ID 2 against the rest is evident, and the higher weights for Q_{c1} and Q_{c2} reveal that as the ID increases, a higher degree of precision is needed and therefore the controller becomes more cautious by producing smaller gains k .

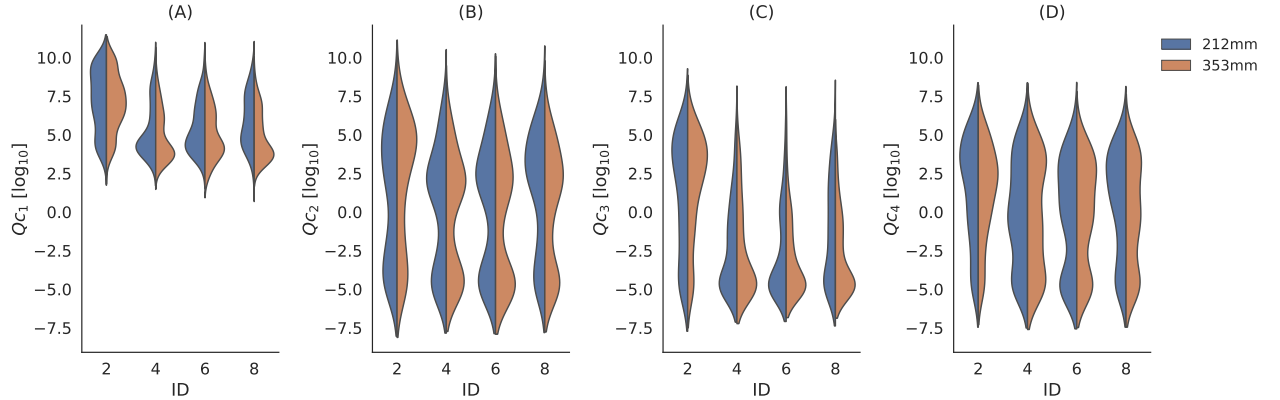


Figure 7: Optimised Q_c parameters for each condition. This figure shows the values of the four elements in the diagonal of matrix Q_c , for all subjects and segmented by ID (horizontal axis). The results for Q_{c1} , Q_{c2} , Q_{c3} and Q_{c4} are shown in A, B, C, and D respectively. The violin plots show the data for the two distances between targets (left, in blue: 212 mm and right, in brown: 353 mm). Q_{c1} has consistently higher values compared to the rest of the elements in Q_c and ID 2 has a different distribution shape than the rest of the conditions

As a result of the LQR method that involves the design matrix Q_c , as shown in (35), a set of controller gains k can be obtained to implement the control law described in (5). Fig. 8 presents the values of each element in k in a log scale, grouped by ID, and displaying side by side the distribution for each target distance in the experiment. It can be seen, by comparison with Fig. 7, that ID 2 still shows higher values for all the elements in k . However, the bimodal distributions of Q_{c2} in Fig. 7B were converted to a single low peak with long tails towards the higher values of k .

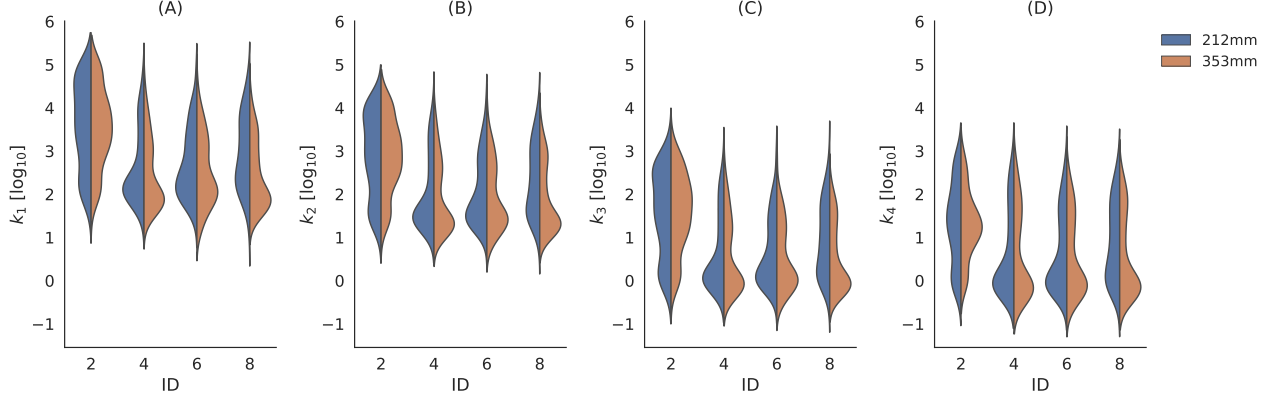


Figure 8: Resulting controller gains \mathbf{k} for each condition. This figure shows the four elements of the gain vector \mathbf{k} for all participants and segmented by ID (horizontal axis). The results for k_1 , k_2 , k_3 and k_4 are shown in A, B, C, and D respectively. Each violin plot presents the results for the two distances between targets (left, in blue: 212 mm and right, in brown: 353 mm) side by side. The controller gains follow a similar trend compared to the design matrix \mathbf{Q}_c from Fig. 7, with ID 2 showing some differences in shape against the rest of the conditions.

8.3 Dynamic responses

The position and velocity RMSE is calculated to give a measure of performance for the optimised controller in each condition according to (37). The results across all participants are shown in Fig. 9. The left figure is the position RMSE for both distances (212 and 353 mm) and the one on the right side corresponds to the velocity RMSE, with the data being grouped according to the ID. In both cases, the error when the distance between left and right targets is 353 mm, is larger compared to the errors registered for 212 mm. The position error is larger in ID 2 for both distances compared to the rest of the conditions, suggesting that the more highly variable behaviour in low constraint cases is harder to model with this particular model. In terms of velocity error, when the task is difficult (i.e. ID 8), the values are smaller compared to the rest of the conditions. This suggests that since more precision is needed due to the target width being reduced, a more cautious regulation is required by the user, in terms of velocity. A similar argument can be made for the position error. In general, the easier conditions (ID 2 in particular) allow a greater degree of error because the targets are wider.

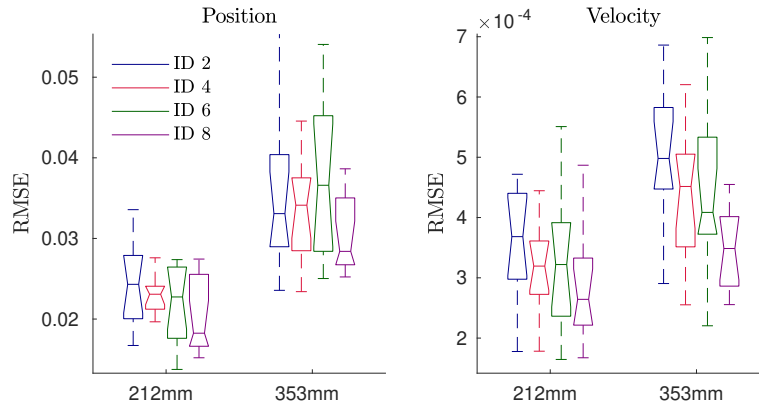


Figure 9: RMSE comparison for the position and the velocity profiles. The left and right figures show position and velocity RMSE respectively. The results in both cases are grouped according to the distance between left and right targets (212 mm and 353 mm, horizontal axis) and also according to the ID of the task, where each box plot represents one of the four conditions of the experiment.

The following figures show the time-series, phase planes and Hooke plots for participant 10, as well as some comparisons made for all participants. Fig. 10 shows the phase planes for ID 8 when the distance between the left and right targets is the shortest (212 mm). This is the most difficult task since the targets are not only close to each other but the target width is also small (0.83 mm). The human response (in blue) tends to fall short of the target (vertical lines in green) and subsequently approaches it via a series of small corrections, as well as overshooting it. The controller

switching strategy described in 7.3 yields trajectories that capture the variability in some regions of the phase planes and it is particularly good at reproducing the trajectories that overshoot the target. This can be seen more evidently in participants 3, 4, 8, 10, and 12. In Fig. 10H, the trajectories that start from the left target depart from small area to then approach the right target, widening and spreading as they get closer.

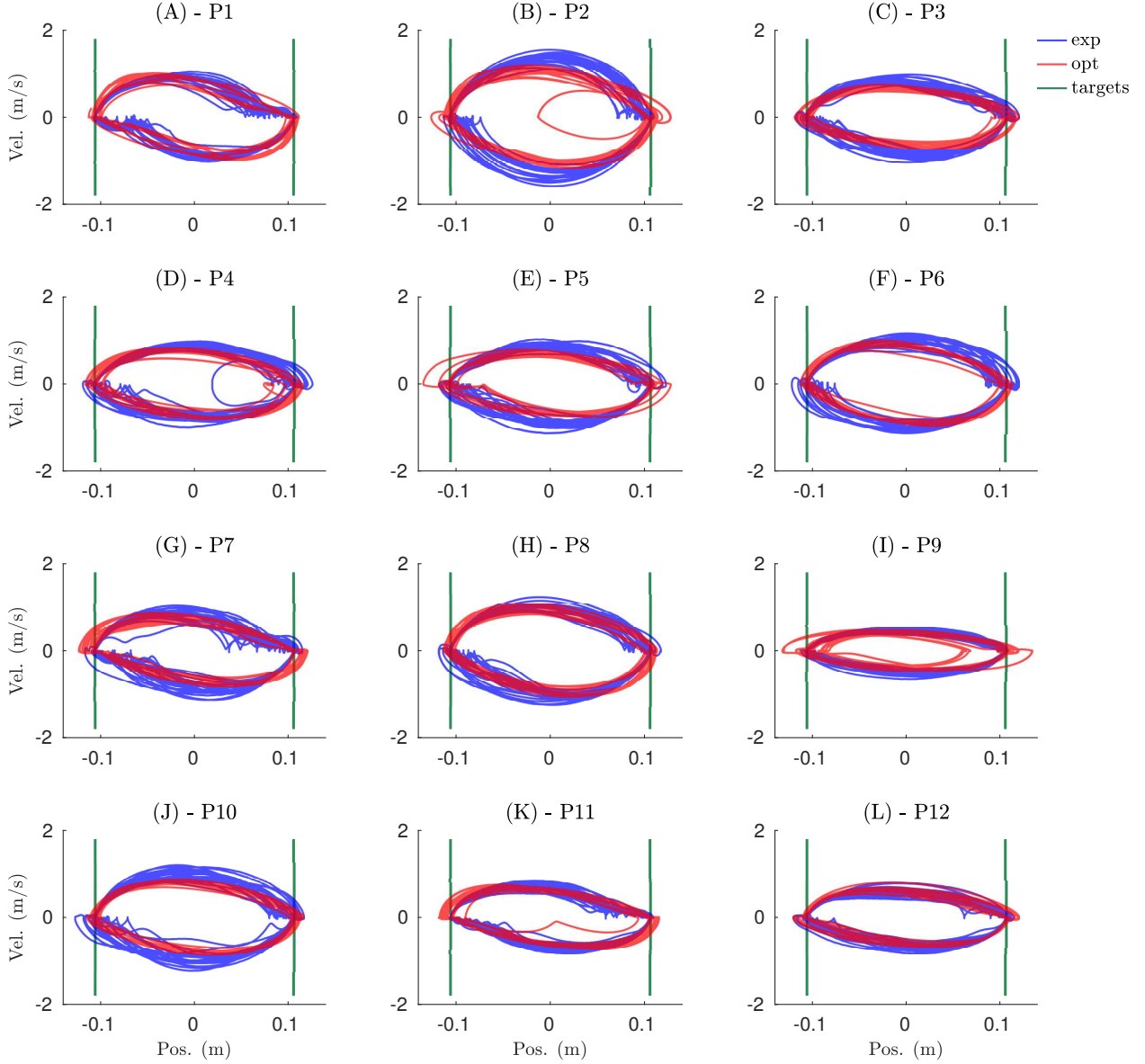


Figure 10: Phase planes for all participants, a distance between targets of 212 mm and an ID of 8. The phase planes compare the pointer position (horizontal axis) against the pointer velocity (vertical axis). The trajectories in blue correspond to the experimental data and the ones in red represent the resulting trajectories when the optimised IC is used. The location of the targets is shown by the vertical lines in green. The optimised IC trajectories capture more of the observed variability when compared with the second order lag model (2ol) responses shown in Fig. 5 for this condition.

In Fig. 11, the phase planes for a distance of 212 mm are shown when the ID is 2 (target width is the largest). The response of the controller is capable of capturing the overall behaviour and some of its associated variability, as the shape of the response changes from a sequence of corrections (Fig. 10) to a more continuous circular movement. In this case, since the difficulty is low, the participants can afford a greater degree of error in the initial portion of the movement leading to trajectories with greater variability and with no correction as they land in the target area. The

controller, in most cases, exhibits trajectories that follow closely the ones generated by each participant. ID 2 is the condition that is substantially different in terms of behaviour than all the rest, as described in Fig. 7A and Fig. 7B.

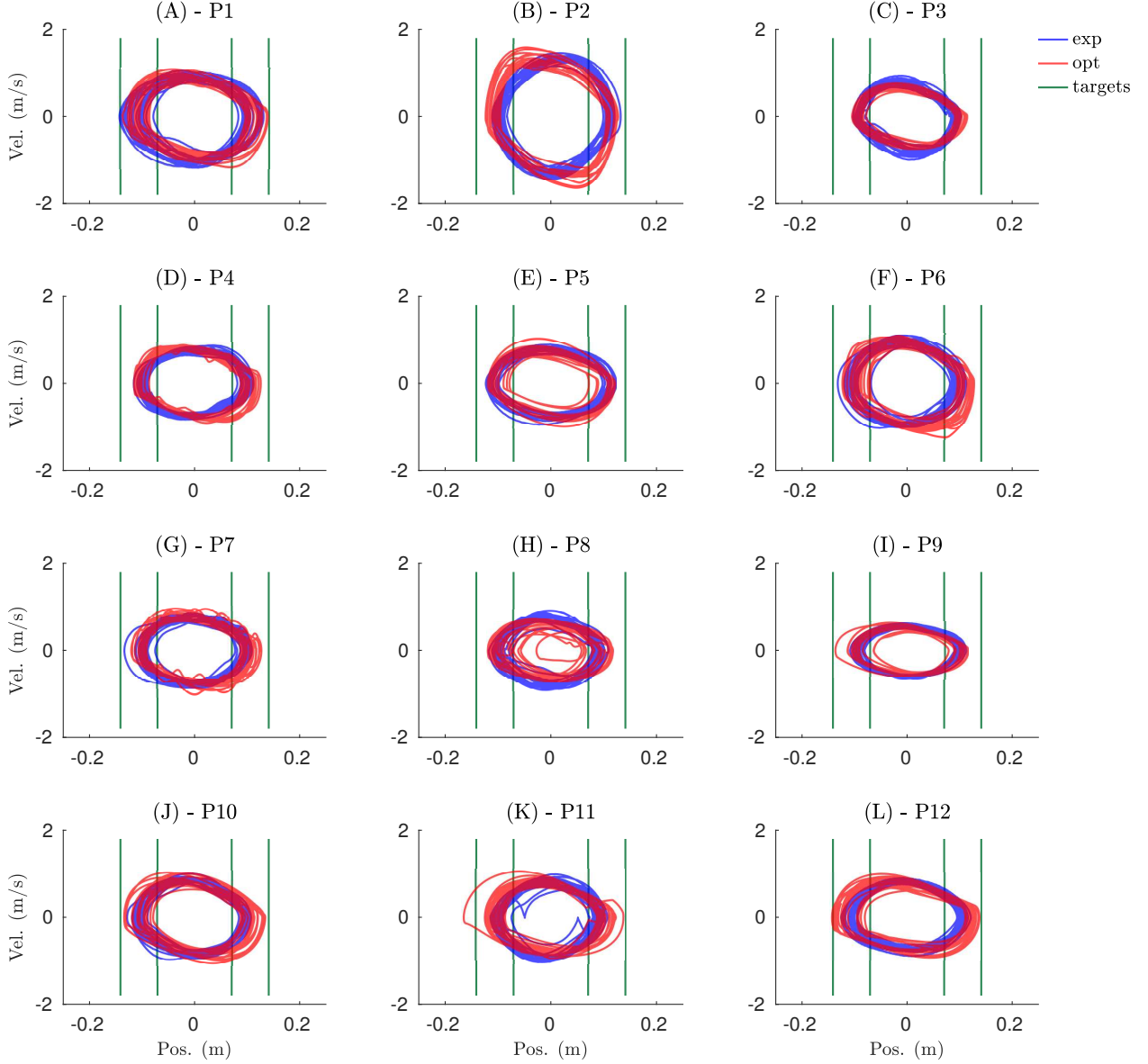


Figure 11: Phase planes for all participants, a distance between targets of 212 mm and an ID of 2. The phase planes compare the pointer position (horizontal axis) against the pointer velocity (vertical axis). The trajectories in blue correspond to the experimental data and the ones in red represent the resulting trajectories when the optimised IC is used. The location of the targets is shown by the vertical lines in green. The optimised phase planes in red follow the shape of the experimental ones, displaying the variability of the trajectory.

In Fig. 12, the time-series associated with the pointer position of participant 10 is shown for the initial part of each trial, where the position recorded from the experiment is in blue, the trajectory generated by the IC is in red, and the target signal (reference) is shown in green. Also, the moments in time when the IC generated an event to trigger the use of feedback are represented by vertical lines in gray.

The left column in Fig. 12 shows data for a distance between left and right targets of 212 mm (A, C, E, G), and the right column shows it for 353 mm (B, D, F, H). Each row in the figure corresponds to a different ID, starting from 2 at the top and ending with 8 at the bottom. It is possible to see how in all conditions, both the experimental and IC trajectories follow the reference closely. In particular, the trajectory generated by the IC exhibits a small degree of error compared to the experimental result, especially as the response approaches the target. Also, for the most difficult

conditions, such as ID 6 or 8 (E, F, G, and H), the position follows a more traditional step response with a small steady-state error. However, the top row shows how the response becomes more similar to a sinusoidal signal due to the quick changes in the target signal in green.

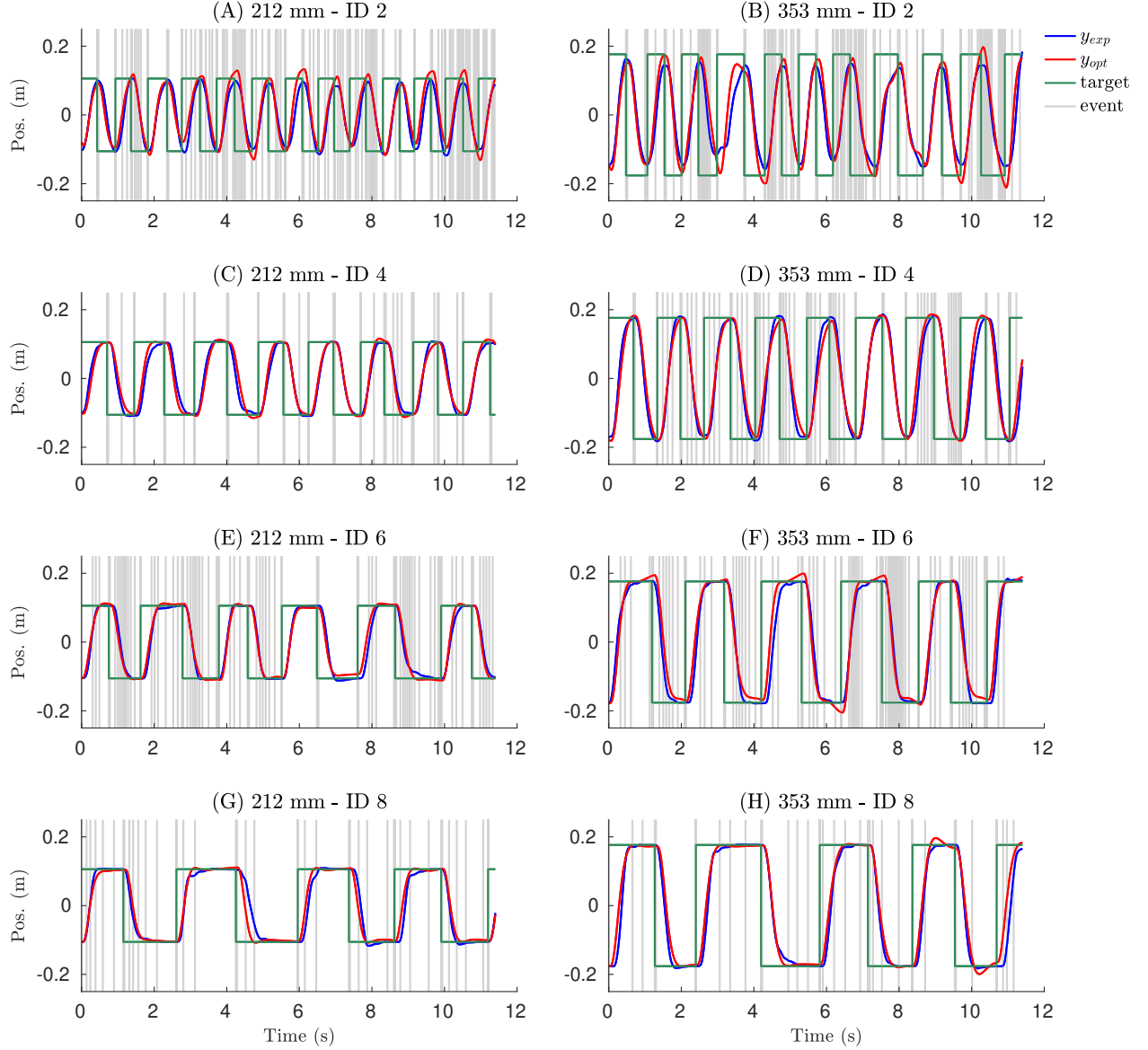


Figure 12: Pointer position for participant 10 in all conditions. Each row corresponds to a particular ID, starting with 2 for the top row and ending with 8 at the bottom. The column on the left shows the pointer position (vertical axis) for a distance between targets of 212 mm (A, C, E, G). The right column shows the same quantities for a distance of 353 mm (B, D, F, H). The horizontal axis shows around 11 seconds of each condition. The participant response y_{exp} is shown in blue, while the trajectories generated by the IC are shown in red as y_{opt} . The target or reference signal is shown in green. The vertical lines in grey show the instances in time when an event was triggered by the optimised IC, signalling the use of feedback. The simulated IC trajectories follow closely the ones generated by the participant; for each change in reference, subtle differences can be seen in the IC trajectories as a consequence of the controller switching approach explained in section 7.3.

IC generates events when the comparison between the hold and the observed states exceeds the specified threshold value as shown in (26). Due to the controller switching strategy described in section 7.3, a different threshold is applied at every change in reference w_c (Fig. 4), which creates different trigger patterns depending on the trial and the model that was selected. This is evident in Fig. 12B and Fig. 12G where the trials around 8 secs exhibit events

that are close in temporal proximity; however, when the next trial starts, the open-loop intervals Δ_{ol} become larger due to the different parameters being applied including a new threshold q value, which results in a slower triggering rate compared to the previous trial. During the time between events, the IC is evolving in an open-loop configuration, using only states that are generated internally by Eq. (14).

Fig. 13 presents the phase planes and Hooke plots of participant 10 for all conditions. The first two columns from left to right contain data for a distance between targets of 212, whereas the third and fourth columns represent a distance of 353 mm. Each row corresponds to a specific ID, starting from ID 2 in the top row and ending with ID 8 at the bottom. In general, the phase planes follow the overall behaviour of the human response (in blue); however, it is possible to see that the IC response (in red) captures the variability seen in the experimental result in all conditions, being slightly less accurate as the difficulty increases.

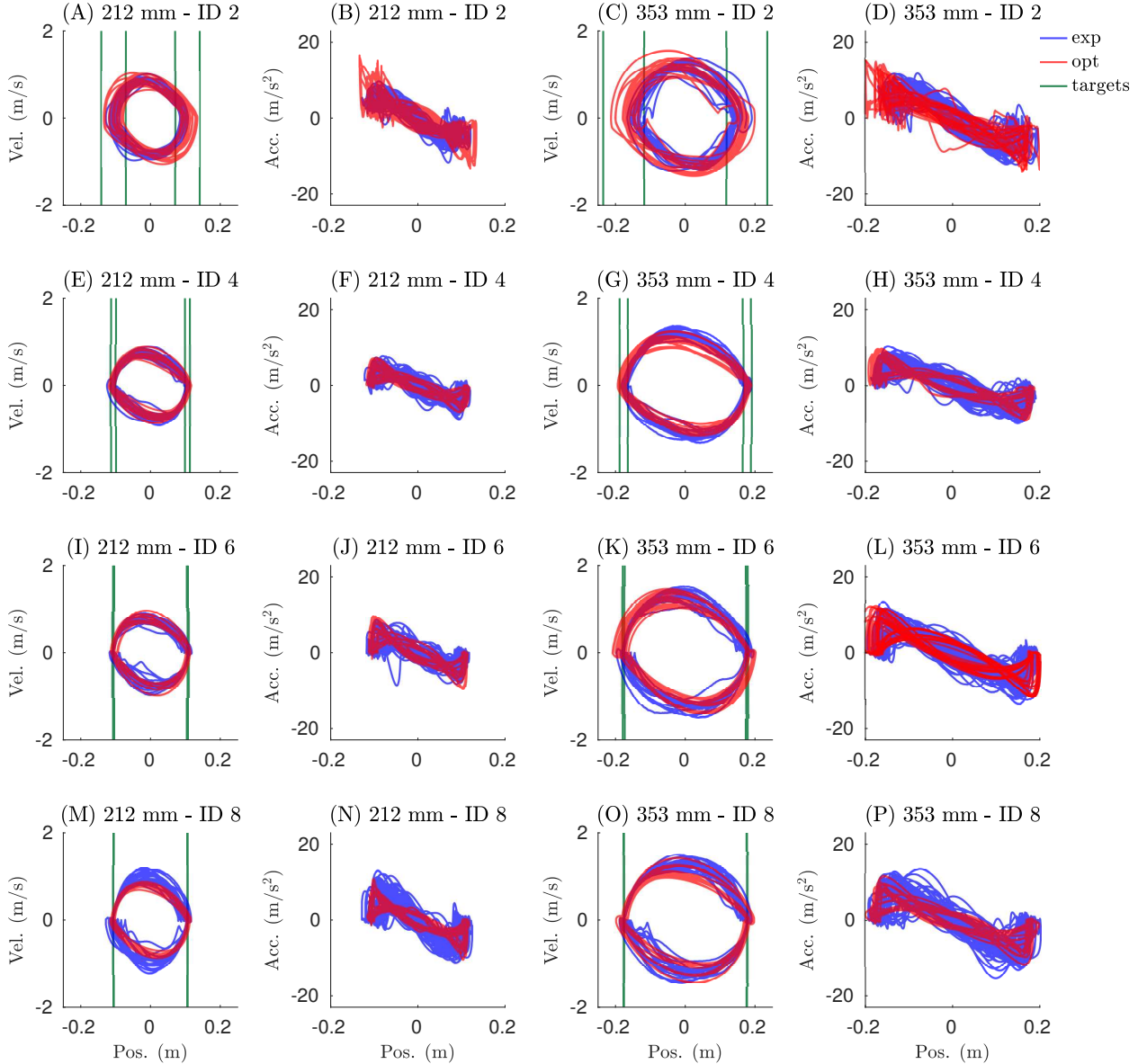


Figure 13: Phase planes and Hooke plots for participant 10 in all conditions. Each row corresponds to a particular ID, starting with 2 for the top row and ending with 8 at the bottom. The two columns on the left show the phase planes (pointer position vs velocity) and Hooke plots (pointer position vs acceleration) for a distance between targets of 212 mm (A, B, E, F, I, J, M, N). The two columns on the right show the same quantities for a distance of 353 mm (C, D, G, H, K, L, O, P). The participant's response is shown in blue, while the trajectories generated by the IC are shown in red. The target or reference signal is shown in green using vertical lines.

The trajectories in Fig. 13E and Fig. 13O, provide some insight into the type of control applied by the participants in these conditions. Once the trajectory approaches the target, the control policy that is used results in a reduction of the pointer velocity accompanied by a sequence of small corrections to reduce the error (more frequent in difficult conditions), or in an error in the opposite direction in the form of overshoot (when the response passes the intended target). For these two cases, the IC output not only covers almost the entire range of possible trajectories generated by this participant, but also reproduces the overshoot behaviour that was previously mentioned. The Hooke plots (second and fourth columns) compare how the pointer acceleration changes with time. In Fig. 13F and Fig. 13P, the acceleration trajectory generated by the IC is smooth (in red), and follows the experimental result (blue) in terms of its overall shape.

8.4 Open-loop intervals

The histograms of the open-loop intervals Δ_{ol} , generated by the intermittent controller, is presented in Fig. 14, where all the Δ_{ol} values for a specific condition were considered for all the participants in the experiment. These values are the actual open-loop intervals recorded from simulation, which can be greater than the minimum open-loop interval Δ_{ol}^{\min} for a particular slice. The minimum open-loop interval Δ_{ol}^{\min} belongs to the set of parameters used in the optimisation approach described in section 8.2, with distributions shown in Fig. 6. In Fig. 14, we decided to overlap both Δ_{ol} and Δ_{ol}^{\min} to show the differences between the two and their relationship with specific conditions of the experiment.

Fig. 14A, C, E, and G, represent the trials where the distance between targets is 212 mm. Similarly, Fig. 14B, D, F, and H, correspond to 353 mm. From top to bottom, each ID is shown as a row, starting with ID 2 at the top (A, B) and ending in ID 8. The values of Δ_{ol} were encapsulated as a histogram (in grey) which shows the frequency of a particular value for a single condition or ID, and its scale is shown on the left y axis of each sub-plot. The values of Δ_{ol}^{\min} are shown as either blue or brown histograms, corresponding to distances between targets of 212 mm and 353 mm respectively.

The results in Fig. 14 show that the majority of the intervals are short in general, having higher frequencies at lower values of Δ_{ol} . Considering Fig. 14A and Fig. 14B, it is clear that histograms in grey decay at a faster rate compared to the rest of the conditions for both distances, showing very few instances of Δ_{ol} beyond 0.25 sec. For ID 4, 6, and 8, the tail of the histogram extends beyond the 0.25 sec consistently, meaning that the open-loop intervals are longer in general compared to the easiest condition of ID 2.

The small values of Δ_{ol} for ID 2 seem to be caused by the effects of the identified threshold q and the mismatch gain \mathbf{A}_p (shown in Fig. 6) and the fact that the IC model had more trouble fitting the response for this particular condition in terms of the target position and velocity, which is displayed in Fig. 9. The RMSE for ID 2 in both distances is larger than the corresponding error in the other conditions, probably as a result of the model trying to capture the variability observed in these trials; however, the poor fit results in low threshold q values which indicates that prediction errors would be addressed by using feedback more often. If the threshold q is low, the triggering patterns of IC would most likely become close to the imposed minimum open-loop interval Δ_{ol}^{\min} , and in some cases triggering would be as fast as the minimum open-loop interval for that particular model would allow.

This behaviour is also affected by the mismatch gain \mathbf{A}_p . Having large values of \mathbf{A}_p means that the control input that is applied to the system is different from the input that would generate the desired performance. Since the input is affected, the states of the system might not reach the specified targets and this would eventually lead to higher triggering rates.

The minimum open-loop intervals Δ_{ol}^{\min} , for both distances, have similar histogram distributions that extend to 0.05 sec approximately. However, the most difficult conditions, i.e., ID 6 and 8, seem to have slightly more values of Δ_{ol}^{\min} around 0.05 than the rest of the conditions. Fig. 14 provides evidence of the interplay between the threshold q and Δ_{ol}^{\min} as well as for the event-driven nature of IC, since even when IC could trigger as fast as Δ_{ol}^{\min} all the time (blue and brown histograms), it does it only after the threshold has been exceeded, leading to the longer open-loop intervals shown by the grey histograms.

9 Densities based on repeated simulations

Using the controller switching strategy from section 7.3, multiple simulations were carried out using the optimised parameters and the associated models in order to create a probability distribution of the IC simulation results, in the phase space. The most basic non-parametric approach to visualise probability densities is simply to binning the data into discrete blocks to create 2D and 3D histograms to expose the variability observed in the data. The availability of such probability density estimates would allow us to predict the likelihood of a given trajectory that a specific participant might take for a particular task. In addition to simple histograms, we can estimate continuous density

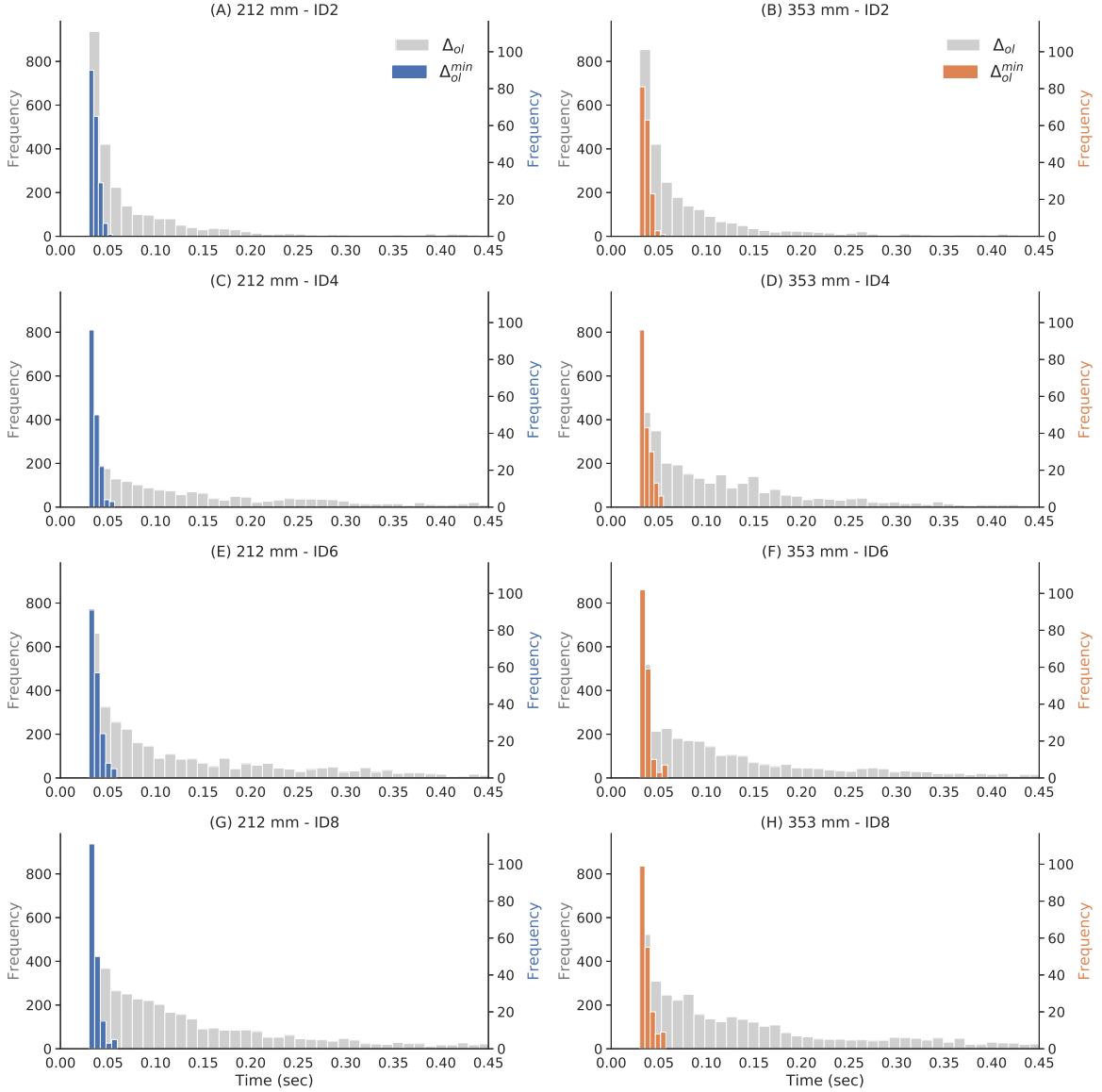


Figure 14: Open-loop interval distributions for all participants. The actual open-loop interval Δ_{ol} , generated by IC, is shown as a grey histogram summarising the data of all participants for a particular condition. Similarly, blue and brown histograms corresponding to the minimum open-loop interval Δ_{ol}^{\min} are shown for a distance between targets of 212 mm and 353 mm respectively. The vertical axis corresponds to the frequency or bin count of a particular value of Δ_{ol} (left axis) and Δ_{ol}^{\min} (right axis). The horizontal axis displays the time in seconds.

functions. In this case, the densities are estimated by *Kernel Density estimates (KDE)*. KDE is a non-parametric approach to estimate the probability density function of a random variable, and is essentially a data smoothing problem where continuous inferences about the population are made, based on a finite data sample (Rosenblatt, 1956; Parzen, 1962). To do this, the first step was to create densities based on the recorded time-series of all the simulations (200 simulations in total), in particular the pointer position and its velocity. With this information, a phase-plane density was created.

To establish a comparison, histograms and KDE densities generated from the experimental data from Participant 10 are presented first, followed by similar visualisations generated from the IC models that were identified. In Fig. 15, a summary of different visualisations of the experimental data is shown, for ID 2 and 8, when a distance between targets is 212 mm. The phase plane is shown for reference (Fig. 15A, E), followed by a 2D histogram representation that was generated based on the phase plane time-series (Fig. 15B, F). These heatmap-like figures in 2D can be extended to obtain a 3D representation as shown in Fig. 15C and Fig. 15G, where the height of each histogram bar represents the bin count in a 30×30 grid. It is possible to observe how, as the phase plane trajectory approaches the targets, the count increases showing areas and bars in a dark blue colour. This is a clear indication of the participant slowing down to land on the target which results in more data points around these areas. Finally, in Fig. 15D and Fig. 15H, a 2D kernel density estimate is generated to have a probabilistic representation of the data.

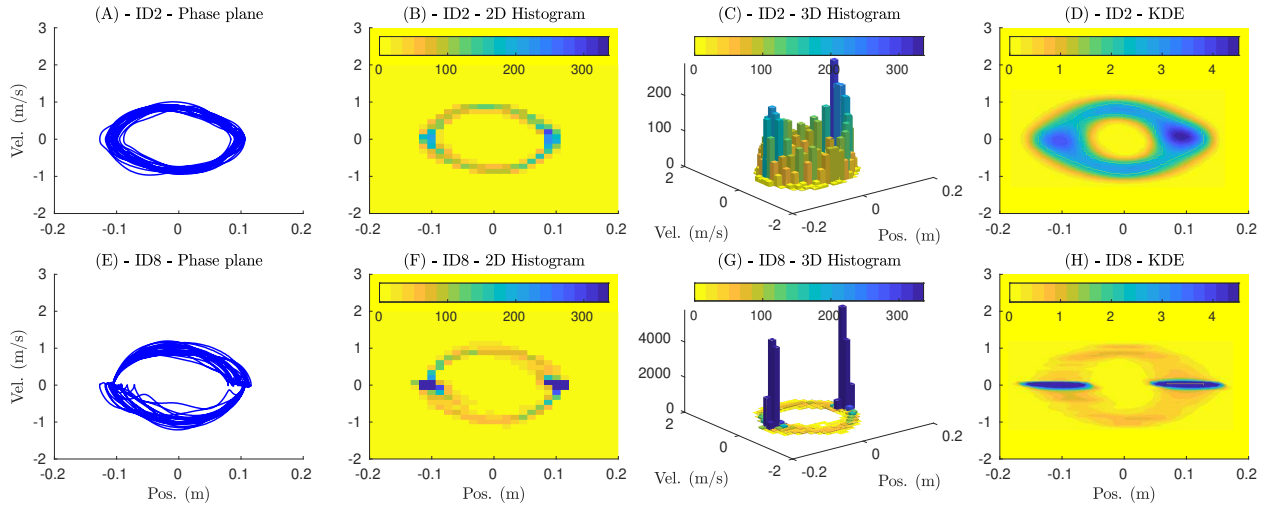


Figure 15: Experimental phase planes, histograms and densities for participant 10 and a distance of 212 mm. (A) shows the recorded phase plane trajectory. (B) is a 2D histogram representation of the phase plane, generated with a grid of 30 by 30 bins. The scale represents the number of data points in each bin. (C) is a 3D histogram where the height of the bars corresponds to bin count, as in the 2D version. (D) is the kernel density estimate of the probability density of the corresponding data. The top row (A, B, C, D) shows data for ID 2, whereas ID 8 is displayed at the bottom (E, F, G, H). The horizontal and vertical axes correspond to pointer position and velocity respectively. For C and G, these two axes appear now in the horizontal plane and the height of the bins in the vertical one.

The identified IC models were used to run 200 simulations using the multiple controller approach to build a density representation. First we show a summary with the corresponding phase plane, 2D-3D histograms and densities for ID 2 and ID 8 for a distance of 212 mm in Fig. 16, which is comparable to Fig. 15, followed by the simulated densities for all distances and conditions (Fig. 17).

The simulated densities show a similar shape to the experimental counterparts, with the variability also present for low ID values such as 2 (A, B). Similarly, the difficult conditions (G and H) also show high density values around the targets showing how the IC model trajectories also spend more time in the vicinity of the target before accelerating in the opposite direction.

9.1 Kullback-Leibler divergence for repeated simulations

The information from the repeated simulations can be used to calculate a distance measure that evaluates how much of the observed experimental distributions is captured by the simulated realisations of the phase planes. To measure the similarity between these, we used a Kullback-Leibler (KL) divergence measure (also called relative entropy). The KL divergence is a measure of how one probability distribution differs from a second, reference probability distribution.

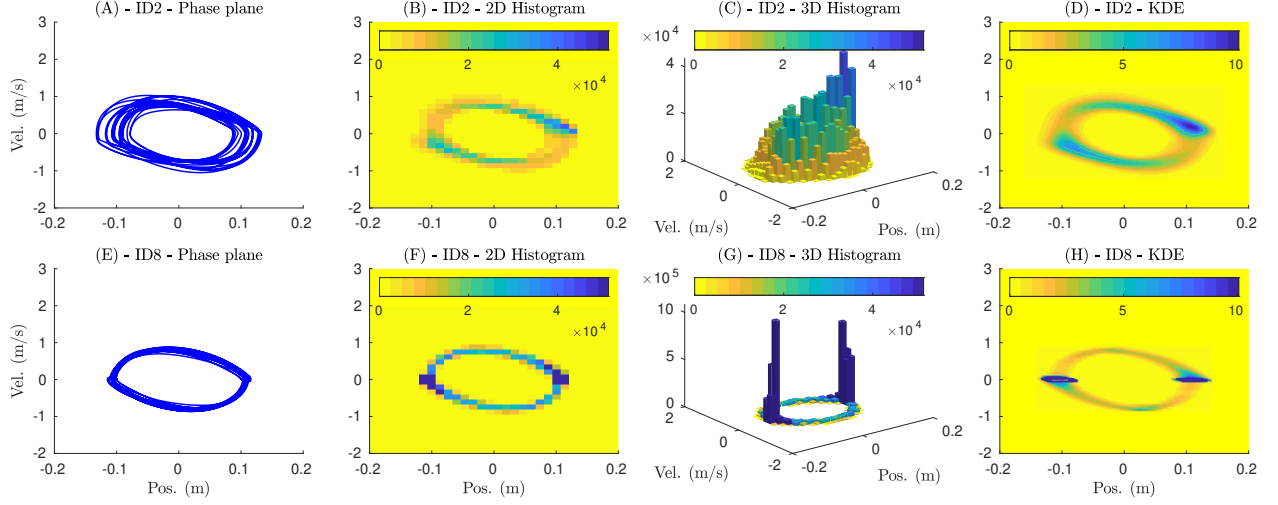


Figure 16: Simulated phase planes, histograms and densities for participant 10 and a distance of 212 mm. A total of 200 simulations, using the multiple controller approach, were used to generate the same type of visualisations as in Fig. 15. The simulated densities have similar shapes to the experimental ones in Fig. 15, showing also higher higher density values around the targets.

For discrete probability distributions P and Q defined on the same probability space, \mathcal{X} , the KL divergence from Q to P is

$$D_{KL}(P||Q) = \int p(x) \log\left(\frac{p(x)}{q(x)}\right) dx, \quad (38)$$

where p and q denote the probability densities of P and Q . We took the approach described in (Wang et al., 2009), using the associated software⁶ to quantify the information loss when compared against the experimental data. We also quantified the loss if the continuous second order lag controller (2ol) (Müller et al., 2017) is used to generate an individual set of simulated trajectories.

The KL divergence values were computed for 20 simulations of the IC, for a distance between targets of 212 mm and for all participants and conditions. To obtain each value, two vectors of samples coming from the simulated time-series of the pointer position and velocity, i.e., the phase plane information, were compared against the corresponding experimental time-series. The reported values for IC represent the mean of the 20 KL values of each simulation run. The mean of the resulting 20 KL values for each participant was computed. This is the reported value IC in Fig. 18, which shows a comparison of the mean KL values over 20 simulation runs of IC and a simulation of the 2ol continuous controller. Each subplot corresponds to a specific ID, starting with ID 2 on the left side (Fig. 18A), ending with ID 8 on the right. The subplots show the KL values on the vertical axis and the two controllers are represented on the horizontal axis (IC on the left, 2ol on the right). The slope of each line (one per participant), shows how different the KL value is for a specific condition. A larger number means that the information loss is greater, therefore a small number indicates that the distribution from the simulation is closer to the observed distribution of the experimental data.

Most lines in Fig. 18 have a positive slope except for two participants (P2 and P4) in ID 2 (Fig. 18A). To gain more insight into the KL-divergence measure, view the phase plane responses for these participants in Fig. 11, which does show repeated divergence in the model behaviour. The positive slopes show the KL divergence for IC are typically lower than for the 2ol controller, indicating a better fit to the distribution. Overall, the divergences for both controllers in ID 2 are smaller compared to the rest of the conditions (Fig. 18B, C, D) in part because although ID 2 results are *more* variable than others, the variability itself is relatively consistent, making it easier to model.⁷ The variability of individual participants can be seen in Fig. 19, again compare the size and variability of divergence with the phase portrait plots for the same participants in Fig. 11. The boxplots give a clear indication that overall the KL divergence tends to be lower for lower IDs, and that more difficult tasks have a higher KL divergence, and a larger variance in that divergence. Overall, the easier tasks result in lower KL values for IC than 2ol for all participants, apart from ID 2 for P2, P4, P5, P8 and P12.

⁶<https://github.com/slaypni/universal-divergence>

⁷Table 2 in the supplementary material contains all the values that were used to obtain Fig. 18.

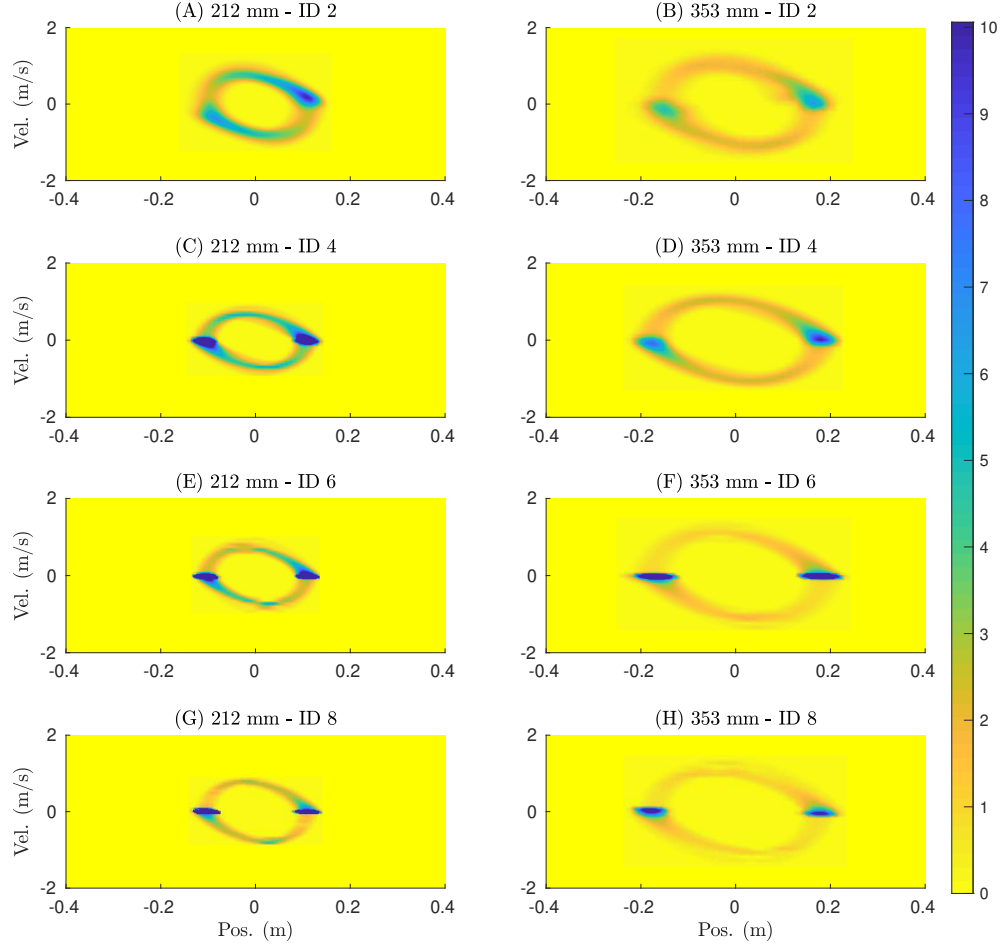


Figure 17: Simulated kernel density estimates for participant 10 in all conditions and distances. (A), (C), (E) and (G) correspond to a distance of 212 mm whereas (B), (D), (F), and (H) are for 353 mm. The different conditions are represented by each row of plots, with ID 2 shown at the top and finishing with ID 8 at the bottom. The horizontal and vertical axes in the figure represent pointer position and velocity respectively. The simulated KDEs have lower values for ID 2 in both distances (A and B) since the participant uses a more cautious approach to hit the target, slowing down considerably, which leads to more data points in these regions.

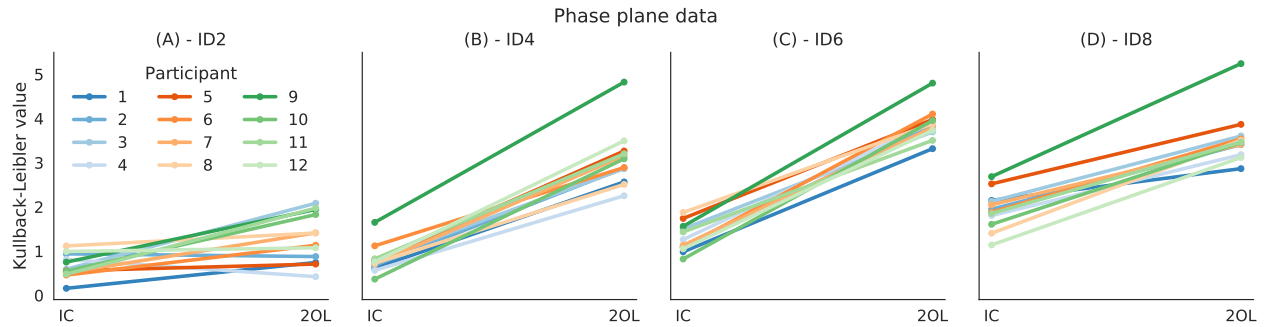


Figure 18: Kullback-Leibler divergence values of IC and 20l controllers. (A), (B), (C), and (D) show the KL value, in the vertical axis, for all participants in conditions ID 2, ID 4, ID 6, and ID 8, respectively. Each line corresponds to a participant, where the left end of the line is the value for IC and the right end point represents the value of the 20l controller. For IC, individual KL values were registered from 20 different simulation runs, from which a mean value was calculated. The mean is reported in this figure. The positive slopes of most of the lines indicate that IC provides a better fit to the observed distribution of the experimental data.

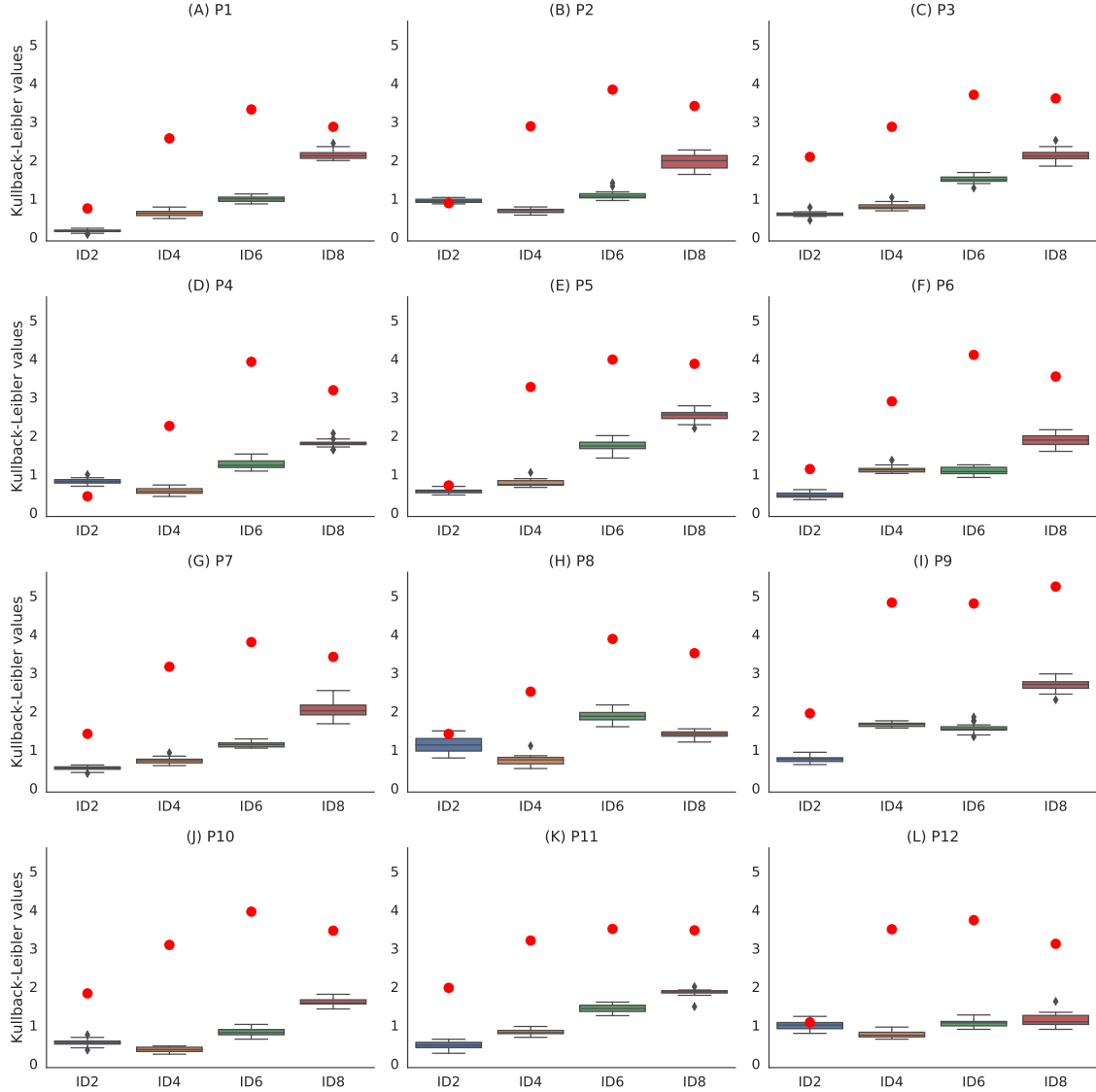


Figure 19: Boxplots of the Kullback-Leibler divergence values for all participants and conditions. The results for each participant are grouped according to the ID of the task (horizontal axis). Overall, the easier tasks result in lower KL values for all participants. Red circles associated with each boxplot represent the value of the 2OL result for a particular condition. If the red dot is above the upper whiskers of the boxplot, this means that it is above the distribution of the IC results, indicating the significance of the difference between the conditions.

10 Low-dimensional visualisations of model structure

While the models may appear complex at first sight, it is possible to explore a simplified model space in two ways: 1. experimentation with optimisation of a reduced subset of model parameters, and 2. use of low-dimensional visualisation techniques to map the full parameter space to one or two dimensions to investigate the range of model behaviour for the different tasks. We combine both approaches in this section.

10.1 Optimisation of a reduced parameter set

Analysis of the variation in model parameters suggested that we could potentially fix some of the values for all users, and restrict the identification process to a subset of parameters. This helps us understand the key factors in the resulting models. We therefore repeated the modelling process described earlier, but restricted the optimisation process to a reduced parameter set, where only \mathbf{Q}_{c1} , \mathbf{Q}_{c2} , q , and \mathbf{A}_p were optimised, leaving out the minimum-open loop interval Δ_{ol}^{\min} , the observer gain \mathbf{Q}_o and the rest of the diagonal entries in \mathbf{Q}_c . The parameters that were left out from the optimisation took the following fixed values: $\mathbf{Q}_o = 10$, $\mathbf{Q}_{c3} = \mathbf{Q}_{c4} = 1$, $\Delta_{ol}^{\min} = 0.3$ sec.

To measure how well the optimisation using a reduced parameter set would compare to the full set optimisation in terms of quality of fit, we decided to evaluate the cost function in (37) for each individual slice. In addition to this, we evaluated the cost function when the controller obtained from each of the slices was simulated against all trials of the condition. Fig. 20 shows the results of this comparison, where Fig. 20A and B show the cost per slice for all participants for the full and reduced parameter sets respectively; similarly, Fig. 20C and D show the cost over all trials for the two sets.

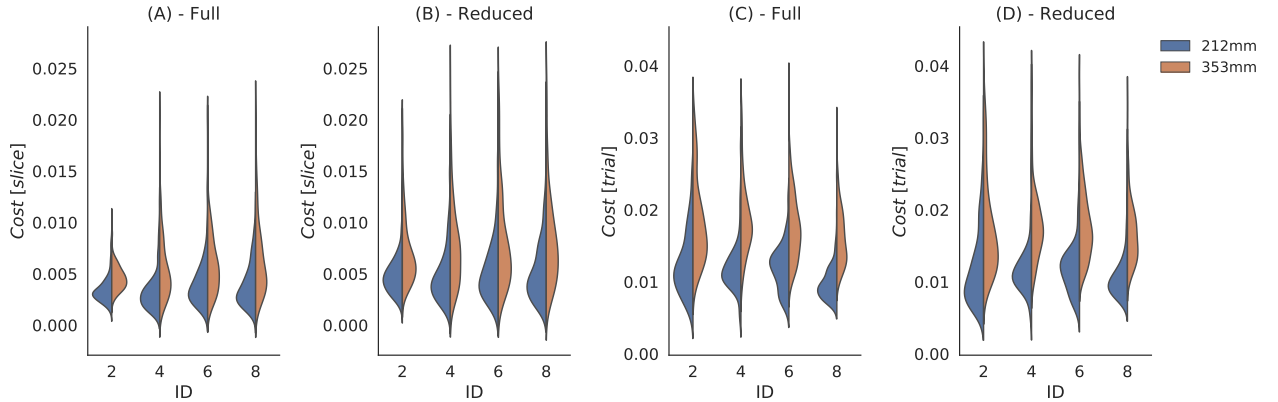


Figure 20: Slice and trial cost for the reduced and full parameter sets in each condition. (A) The cost per slice for the full parameter set, (B) cost per slice for the reduced parameter set, (C) cost over all trials for the full parameter set, and (D) cost over all trials for the reduced parameter set, are shown as violin plots for all participants and categorised by ID on the horizontal axis. The results are also grouped according to the two values of distance between targets used in the experiment (left: 212 mm and right: 353 mm).

From Fig. 20A and B, we can see that the reduced parameter optimisation does not represent too much of a trade off in quality of fit, since the cost per slice values are very similar with the most noticeable difference in ID 2, where the reduced set shows slightly higher cost values. The cost over the entire trials (Fig. 20C, D) for the two sets is very similar in both value and shape of the distributions; however, when compared to the cost per slice, we can see that it is generally higher across all conditions. This is an expected consequence of simulating a single controller against all trials in a condition and the main reason to use the switching control strategy introduced in section 7.3.

The ability to successfully represent the data with only 4 parameters identified from the experimental data, may help reassure readers that the models can capture general properties of pointing behaviours, even in variable conditions such as ID 2, and is not ‘overfitting’ the experimental data. The distributions of these 4 parameters are shown in Fig. 21.

In Fig. 21A, we can see how \mathbf{Q}_{c1} has more compact distributions compared to the same figure for the full set of parameters (Fig. 7A), whereas \mathbf{Q}_{c2} in Fig. 21B still shows elongated bi-modal distributions that are comparable in shape to those in Fig. 7B. The threshold q and the mismatch gain \mathbf{A}_p are shown in Fig. 21C and Fig. 21D respectively. The mismatch gain \mathbf{A}_p in the reduced parameter set has now a longer distribution that spans from -0.1 to 0.1 for ID 2 when compared to its distribution in the full parameter set (Fig. 6B) which is more compact and centered around 0.1.

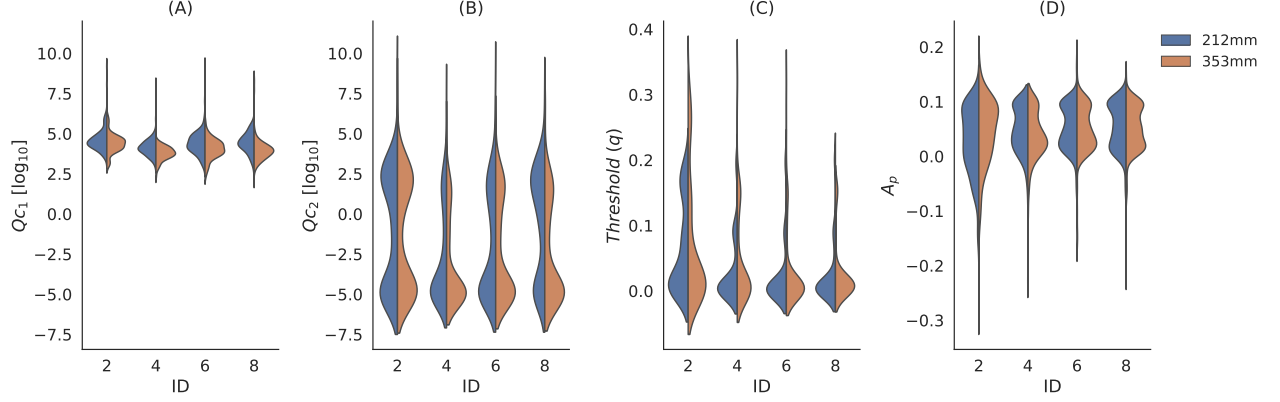


Figure 21: Optimised controller parameters (for a reduced set) for each condition. (A) Q_{c1} , (B) Q_{c2} , (C) the threshold q , and (D) the mismatch gain A_p are shown as violin plots including data of all participants and categorised by ID (horizontal axis). The results are also grouped according to the two values of distance between targets used in the experiment (left: 212 mm and right: 353 mm).

The impact of the optimised Q_c values is on the gain parameters, therefore in Fig. 22 we show all elements of the state-feedback gain vector \mathbf{k} which is computed via LQR using the matrix Q_c as a design parameter.

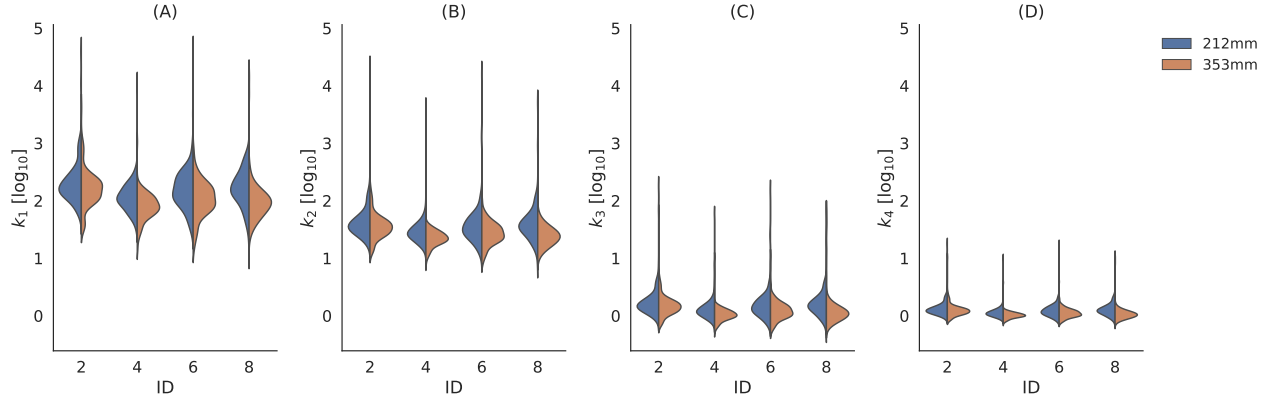


Figure 22: Resulting controller gains \mathbf{k} (for a reduced set) for each condition. This figure shows the four elements of the gain vector \mathbf{k} for all participants and segmented by ID (horizontal axis). The results for k_1 , k_2 , k_3 and k_4 are shown from left to right in A, B, C and D respectively. Each violin plot introduces the results for the two distances between targets (left, in blue: 212 mm and right, in brown: 353 mm) side by side.

The distributions of the state-feedback gain vector \mathbf{k} for the reduced parameter set, shown from left to right in Fig. 22, are more compact when compared to the corresponding gains of the full parameter set optimisation in Fig. 8; on the other hand, the overall trend is similar for both parameter sets where k_1 and k_2 are both higher than k_3 and k_4 , and k_2 being lower in general than k_1 .

10.2 Visualisation of low-dimensional embeddings with UMAP

Traditionally approaches such as Principal Components Analysis (PCA) have been used to visualise reduced dimensional representations of high-dimensional data. PCA is a linear approach, which limits its power. In this section we use a modern nonlinear algorithm, *Uniform Manifold Approximation and Projections (UMAP)* (McInnes et al., 2018), to arrange the reduced, 4-dimensional model parameter vectors on a two-dimensional space. This allows us to visualise the smooth changes in model parameters over the space, as shown in Fig. 23 and helps us associate them with qualitative changes in pointing behaviour, as shown in Fig. 24. This gives an impression of the locations of specific users in parameter space for a given condition, and the impact of different parameters on time-series variability. In general, the individual users have behaviours which are spread widely around the space, with only extreme behaviours (e.g. P2) in more distinct distributions.

In Fig. 23, the resulting two-dimensional embedding obtained using UMAP is displayed, while its samples are coloured according to the value of the two first state-feedback gains \mathbf{k}_1 and \mathbf{k}_2 (A and B), as well as the threshold q and mismatch gain A_p (C and D). This gives insight on how the relevant parameters change in the 2D space. For instance, the samples for \mathbf{k}_1 and \mathbf{k}_2 have higher values in general towards the top left corner of the embedding. The threshold q is generally low except for a patch of samples on the top left corner, and A_p shows the lowest values on the left half of the embedding, specially at the bottom.

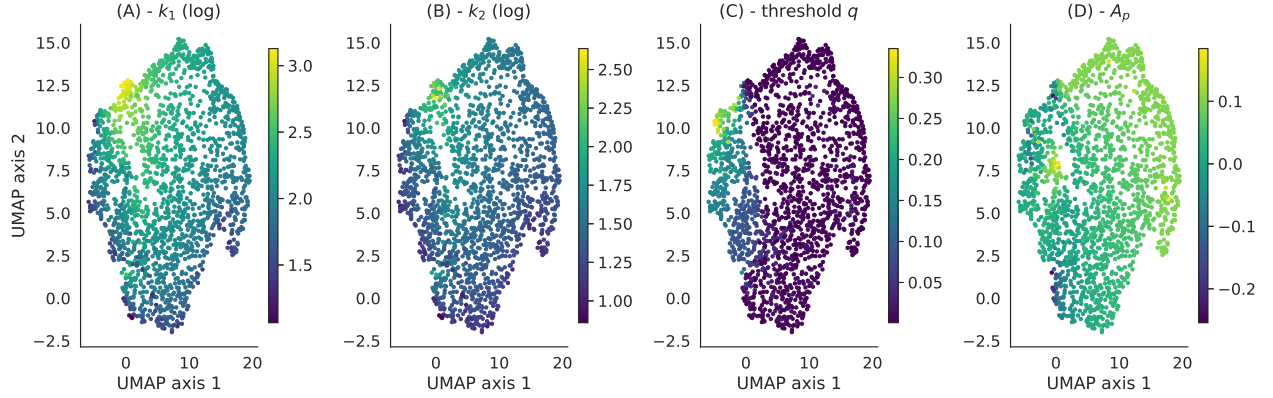


Figure 23: Uniform Manifold Approximation using a 2D embedding, coloured using the value of each parameter. From left to right we have the state-feedback gains \mathbf{k}_1 and \mathbf{k}_2 (A, B), followed by the threshold q and the mismatch gain A_p (C, D). Both axes represent the two dimensions of the UMAP embedding, which contains the data for all participants, IDs and distances between targets. This gives an indication of the typical ranges and combinations of parameters obtained from the reduced set optimisation. \mathbf{k}_1 and \mathbf{k}_2 are higher for the samples in the top left region of the embedding. Low levels of the threshold q are quite common except for a small patch of samples located on the left side of the embedding. The mismatch gain A_p has higher values towards the right side, with a small patch of negative values at the bottom.

From the parameter mappings in Fig. 23, we generated Fig. 24 which displays the type of phase planes that IC would generate for a specific condition and participant, while looking at the position of the associated samples over the space. The two-dimensional UMAP embedding is shown in the centre, and relevant samples of different colours are overlapped. The corresponding phase planes are shown on the left and right columns relating the pointer position against velocity.

Participant 2 (A, blue) is clearly clustered in the upper left corner of the embedding for an ID of 2, which coincides roughly with the high gain \mathbf{k} , high threshold q and low A_p region of the space. The phase plane for participant 2 shows trajectories of high velocity (vertical axis), giving rise to a more round phase plane. If this is compared with participant 5 in pink (B), for the same ID and distance, the phase plane does not show the same level of velocity as participant 2 and the associated samples lie mostly on the bottom left region of the embedding that corresponds to low levels for all of the parameters. This suggests that the state-feedback gains have an effect on the velocity profile of the participants.

In similar fashion, participant 4 (C, green) and 9 (D, light purple) are compared for an ID of 6 on the right column of Fig. 24. A more precise trajectory is observed for both participants since the targets are smaller for this condition, but if we look at their samples on the embedding we can see that participant 4 has samples on both the top right and bottom left sections of the embedding, whereas participant 9 is more localised around the bottom right section. These two participants have a considerable amount of samples in the high mismatch gain A_p regions of the embedding.

The easiest condition, i.e., ID 2, has greater degrees of freedom compared to the rest and separates out participants the most in terms of their position in the 2D embedding. This is shown in Fig. 25, where the samples for all participants are displayed for ID 2 and a distance of 212 mm. Participants 2 (blue), 4 (green), and 6 (red) tend to have clusters of samples in the top left region of the embedding, while participants 9 (light purple) and 12 (brown) tend to be in the lower half. The corresponding phase planes for participants 4, 6, 9 and 12 are shown in Fig. 25A, B, C and D, respectively. The samples for all participants are more mixed for the rest of the conditions ⁸

⁸Fig. 26 shows the 2D UMAP embedding for all participants and conditions, and a distance of 212 mm.

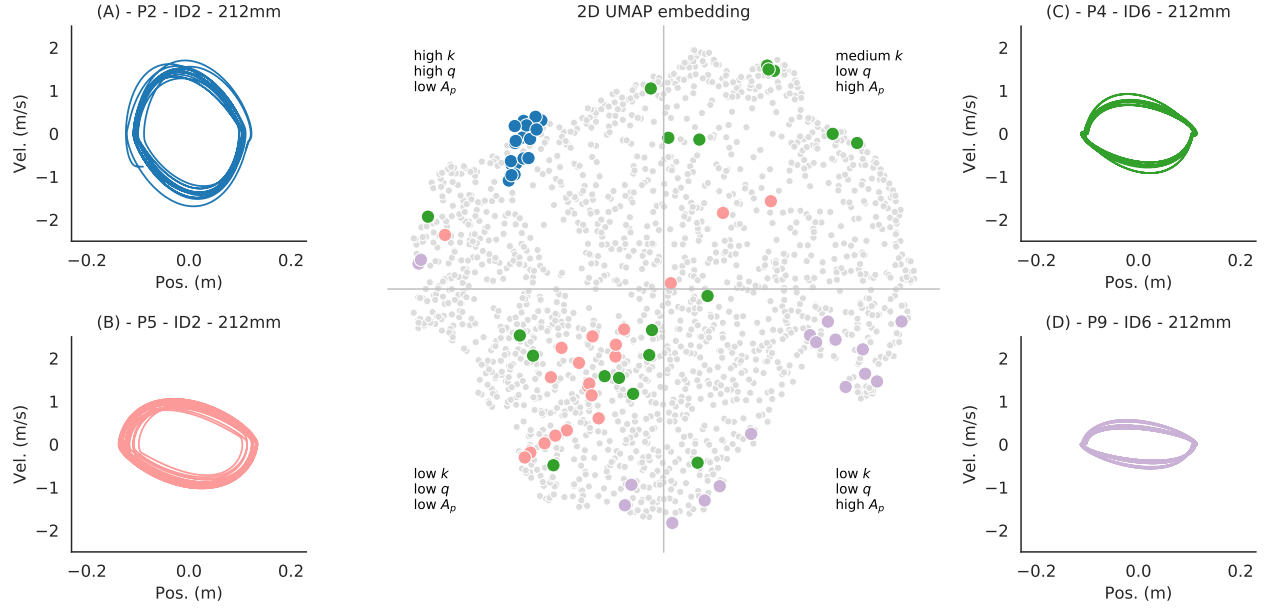


Figure 24: Some samples of individual users and conditions for the 212 mm distance between targets and the associated phase planes. Participants 2 (A, blue) and 5 (B, pink) for an ID of 2 are shown in the left column, while participants 4 (C, green) and 9 (D, light purple) are displayed on the right. The corresponding samples in the 2D UMAP embedding are highlighted using the same colours. The embedding is classified roughly in four regions with approximate features of the optimised parameters, such as high and low values of k , q and A_p . Note how the high variability ID 2 case is in the high gain region, while e.g., the P5 data is spread more evenly in the diagonal axis from low k , low A_p to medium k , high A_p .

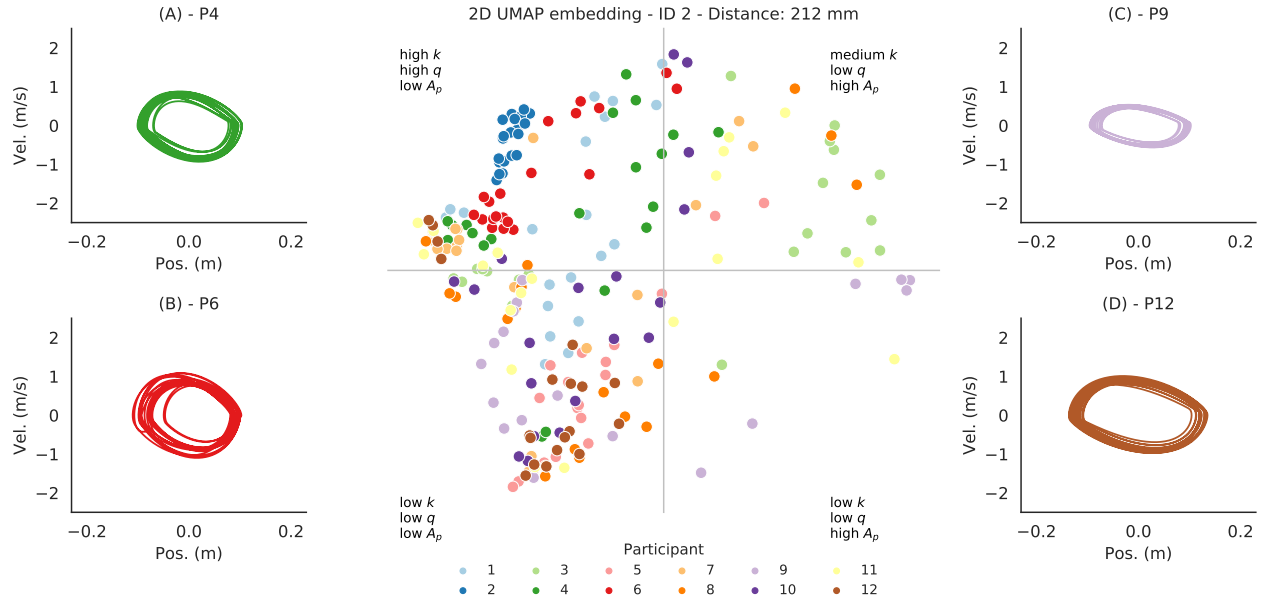


Figure 25: Samples of a 2D UMAP embedding corresponding to all participants, an ID of 2, and a distance of 212 mm. Each participant is shown in a different colour. The embedding is classified roughly in four regions with approximate features of the optimised parameters, such as high and low values of k , q and A_p as in Fig. 24. Participants 2 (blue), 4 (green), and 6 (red) stand out with most samples in the areas of high state-feedback gains k and threshold q , located in the top left region of the embedding. Participants 9 (light purple) and 12 (brown) have most samples in the bottom left region where the values for all parameters are relatively low. The phase planes for participants 4, 6, 9 and 12 are shown in A, B, C and D respectively.

11 Discussion

11.1 Key conceptual advantages of this model

Our results show that intermittent control provides a viable model of mouse movements. In particular, we show that existing continuous control models of mouse movements (e.g., (Müller et al., 2017)), while a significant advance on previous models with no dynamics, provide a highly simplified view of movement dynamics in HCI tasks. In particular, these previous models assume that humans can react to computer feedback continuously. On a high level, humans can appear to react to feedback continuously, such that continuous control models can be viewed as a (rough) approximation of human behavior. However, newer research suggests that humans may not be able to react truly continuously because of the psychological refractory period (Loram et al., 2014). Instead, intermittent control can masquerade as continuous control, such that in some cases both behaviors cannot be distinguished. However, intermittent control is a more general, and more physiologically plausible, explanation of behavior. In particular, it can explain phenomena that can not be explained by continuous control, including the following:

Variability: The parametric, continuous control models proposed in (Müller et al., 2017) are unable to replicate human variability. Instead of replicating the variance of human movements, these models always recreate the same movement given the same initial conditions and task. Continuous control models could be augmented by injecting sensorimotor noise into the control loop to replicate human variability. However, intermittency of control is a physiologically plausible additional noise source (Gollee et al., 2017) that, coupled with the model’s internal dynamics, can explain the variability in pointing movements well.

Submovements: One practical consequence of the simplification associated with continuous control models is their fundamental inability to explain or replicate submovements. While humans demonstrate identifiable submovements in difficult aimed movements, e.g., in mouse pointing, continuous control models predict a single smooth movement towards the target. Submovements are a characteristic feature of aimed movements, and the inability to replicate these represent a fundamental shortcoming of continuous control models. However, this shortcoming is solved through the intermittent control models proposed in this paper. Intermittent control provides a plausible explanation of the physiological mechanisms underlying the existence of submovements, and our work shows that it is also able to replicate movements with submovements empirically. The threshold functions used in this paper are simple fixed levels, but we anticipate that future work can capture more structure by having more complex classifiers which are a function of both the error and the state.

Predictive models in users: One particularly interesting aspect of intermittent control models is that they posit that users maintain an internal model of the computer interface dynamics and predict the feedback they will receive from the computer interface in the future. They only change their control when the received feedback deviates from their internal prediction. This maintenance of an internal model is in line with developments in neuroscience, e.g. (Wolpert and Ghahramani, 2000). More awareness among HCI designers of the fact that control is intermittent and that humans control according to an internal model of the interface dynamics has the potential to fundamentally change the design of the feedback of computer interfaces. Computer interfaces evolve according to an internal state, and aspects of this state are communicated as feedback to the user. The ability of the user to construct an internal model of the state dynamics, as well as to observe the state from feedback is crucial for their ability to close the intermittent control loop more rarely, potentially freeing cognitive resources. Designers of feedback of computer interfaces should pay more attention to making as much as possible of the full state of the computer interface observable, e.g., by visualizing not only the positions but also the velocities of virtual objects. The congruence of feedback received from the interface and the feedback predicted by the user is important not only for the control performance, but also for psychological phenomena such as the agency perceived by the user over the interface (Seinfeld et al., 2020).

Furthermore, IC models previously assumed that the system matched hold was a perfect approximation of the controlled system. In this paper we introduce the concept of the mismatch gain, \mathbf{A}_p , to account for the difference between the internal model (which is used in the hold and in the predictor) and the real system (which is subject to disturbances). This results in the ability of our model to represent the undershooting and overshooting trajectories which are characteristic of this task. We also extend our identification approach to be suitable for a reference tracking task rather than compensatory control, as used previously (Gollee et al., 2017).

11.2 Limitations of the model

This paper presents initial work building on experimental data for one-dimensional pointing tasks of 12 test users in an artificial lab setting, with constant mouse gain, no visual distractors, and a limited range of ID and distance. In particular, our current model formulation assumes linear user interface dynamics, e.g. pointing with constant mouse gain. However, the model can be extended to the case of non-linear user interface dynamics, e.g., non-linear pointing

transfer functions, via effectively local linearisation of a nonlinear observer model. The case of a static non-linearity can be addressed by using its inverse, so that the overall plant appears to be linear. Further directions of future work involve generalising the model to everyday mouse interactions with typical levels of visual distractors on screen, and multivariable movement tasks (e.g. 2D targets of different shapes). However, we anticipate that the nature of the Intermittent Control approach is naturally well-suited to multivariate control models, allowing a flexible expansion to higher-dimensional interaction tasks. Similarly, the dynamic systems roots make it well suited for dynamic tasks such as *Steering law* tasks (Accot and Zhai, 1997), allowing us to better model user behaviour in tunnel or trajectory following tasks, tracking of moving targets (Poulton, 1974) and crossing-based interfaces (Accot and Zhai, 2002). It will also be of use in general gesture recognition models which can often be of significantly higher dimension.

12 Conclusion

We proposed intermittent control models as a model for movement in Human-Computer Interaction, investigating intermittent control of pointing movements with a computer mouse.

We identified parameters of our model from data of a reciprocal pointing experiment. Simulation of our intermittent control model shows that it can replicate human pointing movements well, given a small number of parameters. A significant difference from our previous work on continuous control models in (Müller et al., 2017) is that IC models can both reproduce the empirical variability of human pointing movements and provide a physiologically plausible explanation for the variability, in the system dynamics coupled with the variability of triggering the sampling of feedback information. Intermittent control models are also inherently able to explain and predict submovements. We conclude that for the one-dimensional pointing task, intermittent control models are physiologically plausible and have stronger empirical support than current continuous control models of movement in HCI.

The availability of identifiable, dynamic human control models, which also accurately capture the rich variability of human behaviour, will have an important role in the future design, testing, and analysis of human-computer interaction. While point-and-click interfaces have dominated interaction with computers for decades, they exploit only a tiny fraction of the richness of motion that humans are able to produce. Interfaces that only interpret the movement endpoint at the time of click throw away all information that was generated in the process of movement. This can include using the movement dynamics to give the system predictive information about what user is trying to achieve, what their emotional state is, or user identification, for security or personalisation purposes (the dynamics of movement are much more difficult to counterfeit than, say, the static image of a signature). In the future, interfaces that accumulate information over the whole interaction might go far beyond that. Future interfaces are also tightly integrated in the physical world and equipped with multitudes of sensors such as gyroscopes, accelerometers and cameras. This would enable the interaction to generate richer reactions to the environment and more complex, engaging, dynamics, such as during physical scrolling or layout adjustments, especially in the case of Virtual Reality based on physics-based environment simulations.

The control perspective on interaction provides a unifying theoretical and modelling framework for the description, analysis and model-based design of interfaces. They enable the simulation of user behavior in interaction, reducing the number of user studies necessary in the design phase. Such simulations allow us to gain insight into processes that are difficult to observe because they are internal to the user, and to design and optimize for them.

Funding disclosure

All authors acknowledge funding support from EPSRC grant EP/R018634/1, *Closed-loop Data Science*.

References

- Accot, J. and Zhai, S. (1997). Beyond fitts’ law: Models for trajectory-based hci tasks. In *CHI ’97 Extended Abstracts on Human Factors in Computing Systems*, CHI EA ’97, page 250, New York, NY, USA. Association for Computing Machinery.
- Accot, J. and Zhai, S. (2002). More than dotting the i’s — foundations for crossing-based interfaces. In *Proceedings of the SIGCHI Conference on Human Factors in Computing Systems*, CHI ’02, page 73–80, New York, NY, USA. Association for Computing Machinery.
- Aranovskiy, S., Ushirobira, R., Efimov, D., and Casiez, G. (2016). Modeling pointing tasks in mouse-based human-computer interactions. In *2016 IEEE 55th Conference on Decision and Control (CDC)*, pages 6595–6600.

- Aranovskiy, S., Ushirobira, R., Efimov, D., and Casiez, G. (2020). A switched dynamic model for pointing tasks with a computer mouse. *Asian Journal of Control*, 22(4):1387–1400.
- Bachynskyi, M. (2016). *Biomechanical models for human-computer interaction*. PhD thesis, Universität des Saarlandes Saarbrücken.
- Bachynskyi, M., Palmas, G., Oulasvirta, A., and Weinkauff, T. (2015). Informing the design of novel input methods with muscle coactivation clustering. *ACM Transactions on Computer-Human Interaction (TOCHI)*, 21(6):1–25.
- Balakrishnan, R. (2004). ‘beating’ fitts’ law: virtual enhancements for pointing facilitation. *International Journal of Human-Computer Studies*, 61(6):857–874.
- Barrett, R. C., Selker, E. J., Rutledge, J. D., and Olyha, R. S. (1995). Negative inertia: A dynamic pointing function. In *Conference Companion on Human Factors in Computing Systems*, CHI ’95, page 316–317, New York, NY, USA. Association for Computing Machinery.
- Bays, P. M. and Wolpert, D. M. (2007). Computational principles of sensorimotor control that minimize uncertainty and variability. *The Journal of physiology*, 578(2):387–396.
- Bhushan, N. and Shadmehr, R. (1999). Computational nature of human adaptive control during learning of reaching movements in force fields. *Biological cybernetics*, 81(1):39–60.
- Billon, M., Bootsma, R. J., and Mottet, D. (2000). The dynamics of human isometric pointing movements under varying accuracy requirements. *Neuroscience letters*, 286(1):49–52.
- Blanch, R., Guiard, Y., and Beaudouin-Lafon, M. (2004). Semantic pointing: Improving target acquisition with control-display ratio adaptation. In *Proceedings of the SIGCHI Conference on Human Factors in Computing Systems*, CHI ’04, page 519–526, New York, NY, USA. Association for Computing Machinery.
- Bootsma, R., Fernandez, L., and Mottet, D. (2004). Behind fitts’ law: kinematic patterns in goal-directed movements. *International Journal of Human-Computer Studies*, 61(6):811–821.
- Bye, R. T. and Neilson, P. D. (2008). The BUMP model of response planning: Variable horizon predictive control accounts for the speed-accuracy tradeoffs and velocity profiles of aimed movement. *Human movement science*, 27(5):771–798.
- Card, S. K., Moran, T. P., and Newell, A. (1986). The model human processor: an engineering model for human performance.
- Casiez, G. and Roussel, N. (2011). No more bricolage! methods and tools to characterize, replicate and compare pointing transfer functions. In *Proceedings of the 24th Annual ACM Symposium on User Interface Software and Technology*, UIST ’11, page 603–614, New York, NY, USA. Association for Computing Machinery.
- Casiez, G., Vogel, D., Balakrishnan, R., and Cockburn, A. (2008). The impact of control-display gain on user performance in pointing tasks. *Human-Computer Interaction*, 23(3):215–250.
- Chapuis, O., Blanch, R., and Beaudouin-Lafon, M. (2007). Fitts’ Law in the Wild: A Field Study of Aimed Movements. Technical report, LRI - Laboratoire de Recherche en Informatique, Univ. Paris-Sud. LRI Technical Report Number 1480, Univ. Paris-Sud, 11 pages.
- Cho, S.-J., Murray-Smith, R., and Kim, Y.-B. (2007). Multi-context photo browsing on mobile devices based on tilt dynamics. In *Proceedings of the 9th International Conference on Human Computer Interaction with Mobile Devices and Services*, MobileHCI ’07, pages 190–197, New York, NY, USA. ACM.
- Craik, K. J. (1947). Theory of the human operator in control systems. I. the operator as an engineering system. *British Journal of Psychology*, 38(2):56–61.
- Craik, K. J. (1948). Theory of the human operator in control systems; man as an element in a control system. *The British journal of psychology. General section*, 38(3):142–148.
- Crossman, E. R. F. W. and Goodeve, P. J. (1983). Feedback control of hand-movement and Fitts’ law. *The Quarterly Journal of Experimental Psychology*, 35(2):251–278.
- de C. Hamilton, A. F., Jones, K. E., and Wolpert, D. M. (2004). The scaling of motor noise with muscle strength and motor unit number in humans. *Experimental Brain Research*, 157(4):417–430.
- Dhawale, A. K., Smith, M. A., and Ölvéczky, B. P. (2017). The Role of Variability in Motor Learning. *Annual Review of Neuroscience*, 40(1):479–498.
- Eslambolchilar, P. and Murray-Smith, R. (2004). Tilt-based automatic zooming and scaling in mobile devices – a state-space implementation. In Brewster, S. and Dunlop, M., editors, *Mobile Human-Computer Interaction - MobileHCI 2004*, pages 120–131, Berlin, Heidelberg. Springer Berlin Heidelberg.

- Eslambolchilar, P. and Murray-Smith, R. (2006). Model-based, multimodal interaction in document browsing. In *Proceedings of the Third International Conference on Machine Learning for Multimodal Interaction*, MLMI'06, page 1–12, Berlin, Heidelberg. Springer-Verlag.
- Eslambolchilar, P. and Murray-Smith, R. (2008). Control centric approach in designing scrolling and zooming user interfaces. *International Journal of Human-Computer Studies*, 66(12):838–856.
- Faisal, A. A. and Laughlin, S. B. (2007). Stochastic simulations on the reliability of action potential propagation in thin axons. *PLOS Computational Biology*, 3(5):1–13.
- Faisal, A. A., Selen, L. P. J., and Wolpert, D. M. (2008). Noise in the nervous system. *Nature Reviews Neuroscience*, 9(4):292–303.
- Fekete, J.-D., Elmqvist, N., and Guiard, Y. (2009). Motion-pointing: Target selection using elliptical motions. In *Proceedings of the SIGCHI Conference on Human Factors in Computing Systems*, CHI '09, pages 289–298, New York, NY, USA. ACM.
- Fischer, F., Bachinski, M., Klar, M., Fleig, A., and Müller, J. (2020). Reinforcement learning control of a biomechanical model of the upper extremity.
- Fitts, P. M. (1954). The information capacity of the human motor system in controlling the amplitude of movement. *Journal of Experimental Psychology*, 47(6):381–391.
- Forssell, U. and Ljung, L. (1999). Closed-loop identification revisited. *Automatica*, 35(7):1215–1241.
- Gawthrop, P., Gollee, H., and Loram, I. (2015). Intermittent control in man and machine. In Miskowicz, M., editor, *Event-Based Control and Signal Processing*, Embedded Systems, chapter 14, pages 1–99. CRC press, London.
- Gawthrop, P., Loram, I., Gollee, H., and Lakie, M. (2014). Intermittent control models of human standing: Similarities and differences. *Biol Cybern*, 108(2):159–68.
- Gawthrop, P., Loram, I., Lakie, M., and Gollee, H. (2011). Intermittent control: A computational theory of human control. *Biological Cybernetics*, 104(1-2):31–51.
- Gawthrop, P. and Wang, L. (2007). Intermittent model predictive control. *Proceedings of the Institution of Mechanical Engineers, Part I: Journal of Systems and Control Engineering*, 221(7):1007–1018.
- Gawthrop, P. and Wang, L. (2011). The system-matched hold and the intermittent control separation principle. *International Journal of Control*, 84(12):1965–1974.
- Gawthrop, P. J. and Wang, L. (2008). Towards model-based continuous-time identification of the human balance controller. *IFAC Proceedings Volumes*, 41(2):11612–11617.
- Gawthrop, P. J. and Wang, L. (2009). Event-driven intermittent control. *International Journal of Control*, 82(12):2235–2248.
- Gollee, H., Gawthrop, P. J., Lakie, M., and Loram, I. D. (2017). Visuo-manual tracking: does intermittent control with aperiodic sampling explain linear power and non-linear remnant without sensorimotor noise? *The Journal of physiology*, 595(21):6751–6770.
- Goodwin, G. C., Graebe, S. F., and Salgado, M. E. (2001). *Control System Design*. Prentice Hall, New Jersey, USA.
- Gori, J. (2018). *Modeling the speed-accuracy tradeoff using the tools of information theory*. PhD thesis, Paris Saclay.
- Gori, J., Rioul, O., and Guiard, Y. (2018). Speed-accuracy tradeoff: A Formal Information-Theoretic Transmission Scheme (FITTS). *ACM Transactions on Computer-Human Interaction (TOCHI)*, 25(5):1–33.
- Guiard, Y. (1993). On fitts's and hooke's laws: Simple harmonic movement in upper-limb cyclical aiming. *Acta psychologica*, 82(1):139–159.
- Guiard, Y. and Beaudouin-Lafon, M. (2004a). Fitts' law 50 years later: Applications and contributions from human-computer interaction. *International Journal of Human-Computer Studies*, 61(6):747–750.
- Guiard, Y. and Beaudouin-Lafon, M. (2004b). Target Acquisition in Multiscale Electronic Worlds. *International Journal of Human-Computer Studies*, 61(6):875–905.
- Hollnagel, E. (1999). Modelling the controller of a process. *Transactions of the Institute of Measurement and Control*, 21(4-5):163–170.
- Hollnagel, E. and Woods, D. D. (2005). *Joint cognitive systems: Foundations of cognitive systems engineering*. CRC Press, Boca Raton, USA.
- Jagacinski, R. J. (1977). A qualitative look at feedback control theory as a style of describing behavior. *Human Factors: The Journal of the Human Factors and Ergonomics Society*, 19(4):331–347.

- Jagacinski, R. J. and Flach, J. M. (2003). *Control Theory for Humans: Quantitative approaches to modeling performance*. Lawrence Erlbaum, Mahwah, New Jersey.
- Jones, K. E., Hamilton, A. F. d. C., and Wolpert, D. M. (2002). Sources of Signal-Dependent Noise During Isometric Force Production. *Journal of Neurophysiology*, 88(3):1533–1544.
- Kleinman, D., Baron, S., and Levison, W. (1970). An optimal control model of human response part i: Theory and validation. *Automatica*, 6(3):357–369.
- Kleinman, D. L. (1969). Optimal control of linear systems with time-delay and observation noise. *Automatic Control, IEEE Transactions on*, 14(5):524–527.
- Kratz, S., Brodien, I., and Rohs, M. (2010). Semi-automatic zooming for mobile map navigation. In *Proceedings of the 12th International Conference on Human Computer Interaction with Mobile Devices and Services, MobileHCI '10*, page 63–72, New York, NY, USA. Association for Computing Machinery.
- Levison, W., Baron, S., and Kleinman, D. (1969). A Model for Human Controller Remnant. *Man-Machine Systems, IEEE Transactions on*, 10(4):101–108.
- Loram, I., Gawthrop, P., and Gollee, H. (2015). Intermittent control of unstable multivariate systems. In *Engineering in Medicine and Biology Society (EMBC), 2015 37th Annual International Conference of the IEEE*, pages 1436–1439, USA. IEEE, IEEE.
- Loram, I. D., Gawthrop, P. J., and Lakie, M. (2006). The frequency of human, manual adjustments in balancing an inverted pendulum is constrained by intrinsic physiological factors. *The Journal of physiology*, 577(1):417–432.
- Loram, I. D., Gollee, H., Lakie, M., and Gawthrop, P. J. (2011). Human control of an inverted pendulum: is continuous control necessary? is intermittent control effective? is intermittent control physiological? *The Journal of physiology*, 589(2):307–324.
- Loram, I. D. and Lakie, M. (2002). Human balancing of an inverted pendulum: position control by small, ballistic-like, throw and catch movements. *The Journal of Physiology*, 540(3):1111–1124.
- Loram, I. D., van de Kamp, C., Gollee, H., and Gawthrop, P. J. (2012). Identification of intermittent control in man and machine. *J R Soc Interface*, 9(74):2070–84.
- Loram, I. D., van De Kamp, C., Lakie, M., Gollee, H., and Gawthrop, P. J. (2014). Does the motor system need intermittent control? *Exercise and sport sciences reviews*, 42(3):117–125.
- MacKenzie, I. S. (1992). Fitts’ law as a research and design tool in human–computer interaction. *Human-computer interaction*, 7(1):91–139.
- McInnes, L., Healy, J., and Melville, J. (2018). Umap: Uniform manifold approximation and projection for dimension reduction.
- Meyer, D., Keith-Smith, J. E., Kornblum, S., Abrams, R. A., and Wright, C. E. (1990). Speed-accuracy trade-offs in aimed movements: Toward a theory of rapid voluntary action. In Jeannerod, M., editor, *Attention and Performance XIII: motor representation and control*, pages 173–226. Lawrence Erlbaum Associates, Inc, New Jersey, USA.
- Meyer, D. E., Abrams, R., Kornblum, S., Wright, C. E., and Smith, J. E. (1988). Optimality in human motor performance: ideal control of rapid aimed movements. *Psychological review*, 95(3):340–370.
- Miall, R. C. (1986). Simple or complex systems? *Behavioral and Brain Sciences*, 9(4):734–734.
- Miall, R. C., Weir, D. J., Wolpert, D. M., and Stein, J. F. (1993). Is the cerebellum a smith predictor? *Journal of motor behavior*, 25(3):203–216.
- Milner-Brown, H., Stein, R., and Yemm, R. (1973). The contractile properties of human motor units during voluntary isometric contractions. *The Journal of physiology*, 228(2):285–306.
- Müller, J., Oulasvirta, A., and Murray-Smith, R. (2017). Control theoretic models of pointing. *ACM Trans. on Computer-Human Interaction*, 24(4):27:1–27:36.
- Murray-Smith, R. (2018). Control theory, dynamics and continuous interaction. In Oulasvirta, A., Kristensson, P. O., Bi, X., and Howes, A., editors, *Computational Interaction*, pages 17–42. Oxford University Press, Oxford.
- Navas, T. and Stark, L. (1968). Sampling or intermittency in hand control system dynamics. *Biophysics Journal*, 14:252–302.
- Nielson, P. D. (1999). The intermittency of control movements and the psychological refractory period. *Motor Control*, 3:280–284.
- Oytam, Y., Nielson, P. D., and O’Dwyer, N. (2005). Degrees of freedom and motor planning in purposive movement. *Human Movement Science*, 24:710–730.

- Park, E. and Lee, B. (2020). An intermittent click planning model. In *Proceedings of the 2020 CHI Conference on Human Factors in Computing Systems*, CHI '20, page 1–13, New York, NY, USA. Association for Computing Machinery.
- Parzen, E. (1962). On estimation of a probability density function and model. *Annals of Mathematical Statistics*, 33(3):1065–1076.
- Poulton, E. C. (1974). *Tracking skill and manual control*. Academic Press, New York.
- Quinn, P., Malacria, S., and Cockburn, A. (2013). Touch scrolling transfer functions. In *Proceedings of the 26th Annual ACM Symposium on User Interface Software and Technology*, UIST '13, pages 61–70, New York, NY, USA. ACM.
- Quinn, P. and Zhai, S. (2018). Modeling gesture-typing movements. *Human-Computer Interaction*, 33(3):234–280.
- Ronco, E., Arsan, T., and Gawthrop, P. J. (1999). Open-loop intermittent feedback control: Practical continuous-time GPC. *Iee Proceedings-Control Theory and Applications*, 146(5):426–434.
- Rosenblatt, M. (1956). Remarks on some nonparametric estimates of a density function. *Annals of Mathematical Statistics*, 27(3):832–837.
- Schmidt, R. A., Zelaznik, H. N., and Frank, J. S. (1978). Sources of inaccuracy in rapid movement. In Stelmach, G. E., editor, *Information Processing in Motor Control and Learning*, pages 183 – 203. Academic Press, New York, USA.
- Seinfeld, S., Feuchtner, T., Maselli, A., and Müller, J. (2020). User representations in human-computer interaction. *Human-Computer Interaction*, 0(0):1–39.
- Shadmehr, R. and Mussa-Ivaldi, S. (2012). *Biological learning and control: how the brain builds representations, predicts events, and makes decisions*. Mit Press, Massachusetts, USA.
- Soukoreff, R. W. and MacKenzie, I. S. (2004). Towards a standard for pointing device evaluation, perspectives on 27 years of Fitts' law research in HCI. *International journal of human-computer studies*, 61(6):751–789.
- Telford, C. W. (1931). The refractory phase of voluntary and associative responses. *J. of Exp. Psychol.*, 14:1–36.
- Torczon, V. (1997). On the convergence of pattern search algorithms. *SIAM Journal on optimization*, 7(1):1–25.
- Trendafilov, D. and Murray-Smith, R. (2013). Information-theoretic characterization of uncertainty in manual control. In *Proceedings of the 2013 IEEE International Conference on Systems, Man, and Cybernetics*, SMC '13, page 4913–4918, USA. IEEE Computer Society.
- van de Kamp, C., Gawthrop, P. J., Gollee, H., and Loram, I. D. (2013). Refractoriness in sustained visuo-manual control: Is the refractory duration intrinsic or does it depend on external system properties? *PLoS Comput Biol*, 9(1):e1002843.
- Van Der Kooij, H. and De Vlugt, E. (2007). Postural responses evoked by platform perturbations are dominated by continuous feedback. *Journal of neurophysiology*, 98(2):730–743.
- Van Der Kooij, H. and Peterka, R. J. (2011). Non-linear stimulus-response behavior of the human stance control system is predicted by optimization of a system with sensory and motor noise. *Journal of computational neuroscience*, 30(3):759–778.
- Velloso, E., Carter, M., Newn, J., Esteves, A., Clarke, C., and Gellersen, H. (2017). Motion correlation: Selecting objects by matching their movement. *ACM Transactions on Computer-Human Interaction (TOCHI)*, 24(3):1–35.
- Wang, Q., Kulkarni, S. R., and Verdu, S. (2009). Divergence Estimation for Multidimensional Densities Via $\$k\$$ -Nearest-Neighbor Distances. *IEEE Transactions on Information Theory*, 55(5):2392–2405.
- Williamson, J. and Murray-Smith, R. (2004). Pointing without a pointer. In *CHI '04 Extended Abstracts on Human Factors in Computing Systems*, CHI EA '04, page 1407–1410, New York, NY, USA. Association for Computing Machinery.
- Williamson, J., Murray-Smith, R., and Hughes, S. (2007). Shoogle: Excitatory multimodal interaction on mobile devices. In *Proceedings of the SIGCHI Conference on Human Factors in Computing Systems*, CHI '07, pages 121–124, New York, NY, USA. Association for Computing Machinery.
- Wobbrock, J. O., Cutrell, E., Harada, S., and MacKenzie, I. S. (2008). An error model for pointing based on fitts' law. In *Proceedings of the SIGCHI Conference on Human Factors in Computing Systems*, CHI '08, page 1613–1622, New York, NY, USA. Association for Computing Machinery.
- Wolpert, D. M. and Ghahramani, Z. (2000). Computational principles of movement neuroscience. *Nature neuroscience*, 3(11):1212–1217.

- Wolpert, D. M., Miall, R. C., and Kawato, M. (1998). Internal models in the cerebellum. *Trends in cognitive sciences*, 2(9):338–347.
- Wu, H. G., Miyamoto, Y. R., Castro, L. N. G., Ölveczky, B. P., and Smith, M. A. (2014). Temporal structure of motor variability is dynamically regulated and predicts motor learning ability. *Nature neuroscience*, 17(2):312.

APPENDIX: Supplementary content

This appendix contains the reference Kullback-Leibler values used in 9.1 as a table, followed by the low dimensional visualisations obtained via uniform manifold approximations, for a distance of 212 mm in all conditions, which complements section 10.

Kullback-Leibler divergence table

This section contains a table with the Kullback-Leibler divergence values used in Fig. 18.

Table 2: Kullback-Leibler divergence values of IC and 2ol controllers*

Participant	IC (ID2)	2ol (ID2)	IC (ID4)	2ol (ID4)	IC (ID6)	2ol (ID6)	IC (ID8)	2ol (ID8)
1	0.161	0.745	0.619	2.567	0.987	3.319	2.149	2.867
2	0.941	0.879	0.680	2.881	1.092	3.834	1.950	3.409
3	0.594	2.085	0.796	2.867	1.504	3.700	2.127	3.606
4	0.814	0.425	0.568	2.255	1.264	3.921	1.806	3.183
5	0.556	0.709	0.773	3.267	1.742	3.980	2.523	3.869
6	0.461	1.134	1.121	2.893	1.086	4.103	1.883	3.539
7	0.514	1.415	0.716	3.158	1.134	3.798	2.050	3.414
8	1.120	1.412	0.730	2.510	1.877	3.880	1.406	3.510
9	0.754	1.944	1.652	4.824	1.563	4.801	2.687	5.242
10	0.550	1.829	0.368	3.090	0.824	3.954	1.609	3.460
11	0.480	1.974	0.828	3.204	1.436	3.506	1.853	3.469
12	0.994	1.077	0.759	3.497	1.055	3.734	1.141	3.118

* Divergence values for all participants in conditions ID 2, ID 4, ID 6, and ID 8 are shown. Each row corresponds to a participant and the values for both IC and 2ol are included. For IC, individual divergence values were registered from 20 different simulation runs, from which a mean value was calculated. The mean is reported in this table.

Uniform manifold approximations for a distance of 212 mm

Fig. 26 shows the 2D UMAP embedding for all IDs, a distance between targets of 212 mm, and when the reduced parameter set is used for the optimisation.

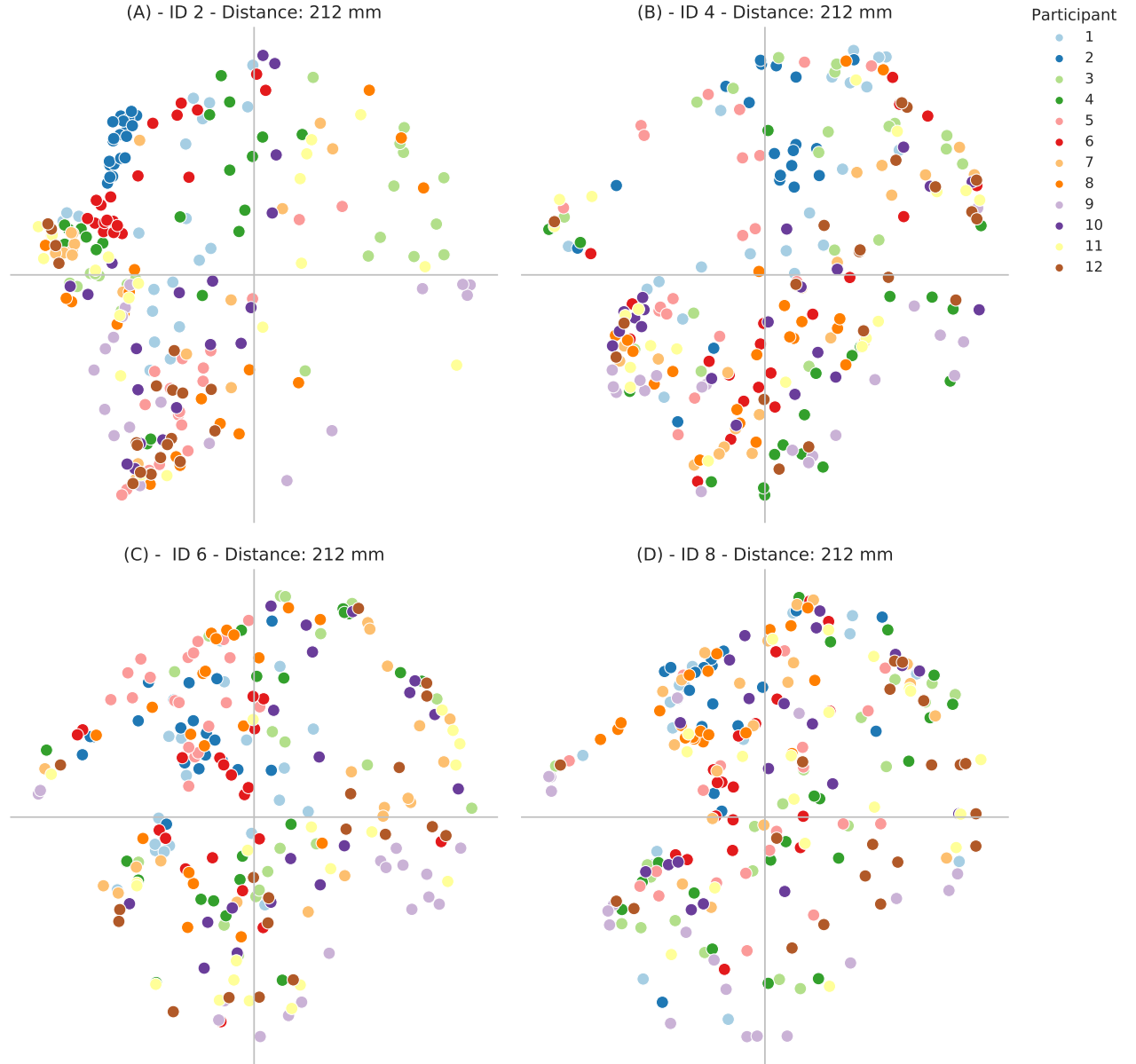


Figure 26: Samples of a 2D UMAP embedding corresponding to all participants and conditions for the 212 mm distance between targets. Each participant is shown in a different colour. The embedding is classified roughly in four regions with approximate features of the optimised parameters, such as high and low values of \mathbf{k} , q and \mathbf{A}_p as in Fig. 24. (A) and (B) at the top contain the samples for ID 2 and 4 respectively, (C) and (D) show the samples for ID 6 and 8. ID 2 stands out with small clusters for participant 2 (blue) and 6 (red). For the rest of the conditions, the samples tend to be more mixed.

Further data visualisations

The following code repository was created as an online appendix of this paper:

https://bitbucket.org/6Albert/ic_point/src/master/.